Development/Plasticity/Repair

Mature Purkinje Cells Require the Retinoic Acid-Related Orphan Receptor-α (RORα) to Maintain Climbing Fiber Mono-Innervation and Other Adult Characteristics

Xiao Ru Chen,[1,2] Nicolas Heck,[3] Ann M. Lohof,[1,2] Christelle Rochefort,[1,2] Marie-Pierre Morel,[1,2] Rosine Wehrlé,[1,2] Mohamed Doulazmi,[1,2] Serge Marty,[4] Vidjeacoumary Cannaya,[1,2] Hasan X. Avci,[1,2] Jean Mariani,[1,2,5] Laure Rondi-Reig,[1,2] Guilan Vodjdani,[6] Rachel M. Sherrard,[1,2] Constantino Sotelo,[7] and Isabelle Dusart[1,2]

[1]UPMC Université Paris 06, UMR 7102, 75005 Paris, France, [2]CNRS, UMR 7102, 75005 Paris, France, [3]UPMC Université Paris 06, CNRS UMR7224/Institut National de la Santé et de la Recherche Médicale UMRS952, 75005 Paris, France, [4]Institute of Biology of the Ecole Normale Supérieure, Inserm U1024, CNRS UMR8197, 75005 Paris, France, [5]Institut de la Longévité, Hôpital Charles Foix, 94205 Ivry sur Seine, France, [6]Centre de Recherche du Cerveau et de la Moelle Epiniere, UPMC/CNRS UMR7225/Institut National de la Santé et de la Recherche Médicale UMRS975, 75013 Paris, France, and [7]Cátedra de Neurobiología del Desarrollo "Remedios Caro Almela," Instituto de Neurociencias, Universidad Miguel Hernández–Consejo Superior de Investigaciones Científicas, 03550 San Juan de Alicante, Spain

Neuronal maturation during development is a multistep process regulated by transcription factors. The transcription factor RORα (retinoic acid-related orphan receptor α) is necessary for early Purkinje cell (PC) maturation but is also expressed throughout adulthood. To identify the role of RORα in mature PCs, we used Cre-lox mouse genetic tools *in vivo* that delete it specifically from PCs between postnatal days 10–21. Up to 14 d of age, differences between mutant and control PCs were not detectable: both were mono-innervated by climbing fibers (CFs) extending along their well-developed dendrites with spiny branchlets. By week 4, mutant mice were ataxic, some PCs had died, and remaining PC soma and dendrites were atrophic, with almost complete disappearance of spiny branchlets. The innervation pattern of surviving RORα-deleted PCs was abnormal with several immature characteristics. Notably, multiple functional CF innervation was reestablished on these mature PCs, simultaneously with the relocation of CF contacts to the PC soma and their stem dendrite. This morphological modification of CF contacts could be induced even later, using lentivirus-mediated depletion of *rora* from adult PCs. These data show that the late postnatal expression of RORα cell-autonomously regulates the maintenance of PC dendritic complexity, and the CF innervation status of the PC (dendritic vs somatic contacts, and mono-innervation vs multi-innervation). Thus, the differentiation state of adult neurons is under the control of transcription factors; and in their absence, adult neurons lose their mature characteristics and acquire some characteristics of an earlier developmental stage.

Introduction

Transcription factors drive the developmental acquisition of mature neuronal features (Polleux et al., 2007; Hobert, 2011). Some of these transcription factors maintain their expression into adulthood. The exact role of this adult expression is not clear, but in some cases they are required to maintain adult neuronal characteristics. For example, the removal of Pet-1 or Nurr1 in the adult mouse nervous system results in a progressive loss of serotonergic or dopaminergic neuron function, respectively (Kadkhodaei et al., 2009; Liu et al., 2010). The present study was undertaken to investigate whether the transcription factor retinoic acid-related orphan receptor α (*rora*, RORα, NR1D1), a member of the nuclear hormone-receptor superfamily, is necessary for the maintenance of adult Purkinje cell (PC) characteristics.

The expression of RORα in PCs starts very early in development and continues during adulthood (Ino, 2004). In spontaneous mutant (*staggerer*) or *rora* knock-out mice, most of the Purkinje cells die within the first month of life (Herrup and Mullen, 1979; Dussault et al., 1998; Vogel et al., 2000; Doulazmi et al., 2001). In addition, surviving PCs do not develop spiny branchlets, remaining in an immature morphological state (Landis and Sidman, 1978; Sotelo, 1978; Boukhtouche et al., 2006b). RORα is necessary for the retraction of transient PC dendrites early in development to allow the establishment of a mature dendritic tree (Boukhtouche et al., 2006b). Furthermore, studies of *rora*-

Received June 22, 2012; revised April 20, 2013; accepted April 26, 2013.

Author contributions: X.R.C., A.M.L., J.M., L.R.-R., C.S., and I.D. designed research; X.R.C., N.H., A.M.L., M.-P.M., R.W., V.C., S.M., A.X.H., R.M.S., and I.D. performed research; G.V. contributed unpublished reagents/analytic tools; X.R.C., N.H., A.M.L., C.R., M.-P.M., R.W., M.D., S.M., R.M.S., C.S., and I.D. analyzed data; X.R.C., A.M.L., R.M.S., C.S., and I.D. wrote the paper.

This work was supported by the CNRS, UPMC, and ANR-07-NEURO-043–01. C.S. was supported in part by the Spanish Ministry of Science and Innovation Grant BFU2010–27326. We thank Richard Schwartzmann (Plateform Imagerie, IFR83) and David Godefroy (Cellular Imaging Facility of the Institut de la Vision, Paris) for help with confocal and Nanozoomer slides scanning, respectively.

The authors declare no competing financial interests.

Correspondence should be addressed to Dr. Isabelle Dusart, Equipe Différenciation Neuronale et Gliale, NPA UMR7102, Université Pierre et Marie Curie, Bat B, 6eme, Case 12, 9 Quai Saint Bernard, 75005 Paris, France. E-mail: isabelle.dusart@snv.jussieu.fr.

DOI:10.1523/JNEUROSCI.2977-12.2013

 0270-6474/13/339546-17$15.00/0

deficient models have suggested some roles for RORα in the adult PC: adult *rora* haploinsufficient mice show premature dendritic atrophy compared with wild-type mice and also show earlier PC loss (Zanjani et al., 1992; Hadj-Sahraoui et al., 1997; Doulazmi et al., 1999; Janmaat et al., 2011). However, it is unknown whether these effects are the result of RORα deficiency in the adult or the cumulative effect of a reduced amount of RORα throughout development.

To address the role of RORα in mature PCs, we developed a mouse model in which the *rora* gene is deleted specifically in PCs between the 10th and 21st postnatal day. At 2 weeks of age, PCs in mutant and control mice have acquired most of their adult characteristics, including a complex dendritic tree with many tertiary branchlets, parallel fiber (PF) synapses, and climbing fiber (CF) mono-innervation as well described previously (for review, see Sotelo and Dusart, 2009; Kano and Hashimoto, 2009; van Welie et al., 2011). The loss of RORα from PCs at this relatively late stage of their maturation was associated with dendritic retraction, almost complete loss of spiny branchlets, new CF multi-innervation, and the appearance of perisomatic spines, suggesting regressive changes with a reversal of developmental processes. The effects of deleting PC *rora* even later in adulthood corroborated these observations. Our findings indicate that continued expression of the transcription factor RORα is necessary after neuronal maturation to maintain mature morphological and innervation characteristics in the adult PC. In the absence of RORα, PCs develop immature characteristics, including CF multi-innervation, suggesting that maintaining the state of differentiation of adult neurons is under the control of transcription factors.

Materials and Methods

Animals. All procedures were submitted and approved by the Regional Ethics Committee in Animal Experiment 3 of Ile-de-France region (p3/2009/020). Animals had *ad libitum* access to food and water with 12 h light-dark cycle. C57BL/6 mice homozygous for the floxed *Rora* allele ($Rora^{fl/fl}$) (Clinique de la Souris; see Fig. 1*A*) were crossed with C57BL/6 heterozygous ($Pcp2$::$Cre^{+/-}$) mice, expressing Cre under the control of the *Pcp2* (L7) promoter (B6.129-Tg(Pcp2::Cre)2Mpin, The Jackson Laboratory; see Fig. 1*A*) to generate $Pcp2$::$Cre^{+/-}$;$Rora^{fl/+}$ and $Pcp2$::$Cre^{-/-}$;$Rora^{fl/+}$ mice. Mating these mice yielded the parent mice used in our study: $Pcp2$::$Cre^{+/-}$;$Rora^{fl/+}$, $Pcp2$::$Cre^{-/-}$;$Rora^{fl/+}$, $Pcp2$::$Cre^{+/-}$;$Rora^{fl/fl}$, and $Pcp2$::$Cre^{-/-}$;$Rora^{fl/fl}$. A YFP$stop^{fl/fl}$ reporter mouse in which a stop signal is flanked by two loxP sites was also used (Srinivas et al., 2001). By crossing YFP$stop^{fl/fl}$ mice with $Rora^{fl/fl}$, we generated another line of parent mice YFP$stop^{fl/fl}$;$Rora^{fl/fl}$.

For the behavior experiments, we used male littermates derived from crosses between $Pcp2$::$Cre^{+/-}$;$Rora^{fl/+}$ and $Pcp2$::$Cre^{-/-}$;$Rora^{fl/+}$ to obtain within the same litters the mutant $Pcp2$::$Cre^{+/-}$;$Rora^{fl/fl}$ (mutant) and the three types of control: $Pcp2$::$Cre^{-/-}$;$Rora^{+/+}$ (wild-type control: WT), $Pcp2$::$Cre^{+/-}$;$Rora^{+/+}$ (L7-Cre control: L7CTRL), and $Pcp2$::$Cre^{-/-}$;$Rora^{fl/fl}$ (floxed *Rora* control: RORCTRL).

For the immunohistochemistry studies, $Pcp2$::$Cre^{+/-}$;$Rora^{fl/fl}$ and $Pcp2$::$Cre^{-/-}$;$Rora^{fl/fl}$ were mated to obtain the male mutant mice and their male littermate controls.

For the electrophysiology experiments, to visualize the mutant Purkinje neurons, the parent mice YFP$stop^{fl/fl}$;$Rora^{fl/fl}$ and $Pcp2$::$Cre^{+/-}$;$Rora^{fl/fl}$ were crossed to obtain $Pcp2$::$Cre^{-/-}$;YFP$stop^{fl/fl}$;$Rora^{fl/fl}$ as control and $Pcp2$::$Cre^{+/-}$;YFP$stop^{fl/fl}$;$Rora^{fl/fl}$ as mutant. Mice of both sexes (P15–P16) and males of 1 month of age were used for these experiments.

For the Cre-expressing lentiviral vector injection studies, $Rora^{fl/fl}$ or YFP$stop^{fl/fl}$; $Rora^{fl/fl}$ male mice of 2 months of age were used.

Mice were genotyped by PCR using genomic DNA prepared from mouse tails by incubating in 60 μl of 25 mM NaOH/0.2 mM EDTA at 95°C for 30 min followed by 5 min at 4°C, then neutralizing the mixture by adding 60 μl of 40 mM Tris, pH 8.1, or 5 μl of the sample was used in each genotyping PCR according to the final volume (20 or 25 μl). Different primer pairs were used for PCR to identify the different alleles.

Two pairs of primers were used for identifying floxed *rora* allele: 5′-AGAGCAATGCCACCTACTCCTGTCC-3′ and 5′-AGTACAGGACACTTCGGTGTC-3′ for one loxP site, and 5′-TTGTGTATACCACCACAAGTGCACC-3′ and 5′-CTAATCCTCCATCCCTTACAC-3′ for the other loxP site; one for L7Cre allele 5′-CGATGCAACGAGTGATGAGG-3′ and 5′-GCATTGCTGTCACTTGGTCGT-3′, and 3 primers for YFP allele 5′-AAAAGTCGCTCTGAGTTGTTAT-3′, 5′-GGAGCGGGAGAAATGGATATG-3′, and 5′-GCCAAGAGTTTGTCCTCAACC-3′.

PCR cycling was initiated by a denaturation at 95°C for 5 min, then an amplification through 35 cycles of 30 s at 95°C, 30 s at Tm of primers, and 30 s at 72°C, followed by10 min at 72°C. The Tm of floxed *rora*, *Pcp2*::Cre, and YFP primers are 60°C, 58°C, and 62°C respectively.

Behavior study. All behavioral studies were performed blind to the genotype of mice. All animals were tested according to the SHIRPA protocol (Rondi-Reig et al., 2001; Rondi-Reig and Mariani, 2002). Animals were kept isolated throughout behavioral experiments and from 7 d before, to limit the variability resulting from social interaction. The tests aimed to detect potential differences in sensorimotor control performances. Mice were first positioned at the center of an arena made of gray perspex (45 × 45 cm) surrounded by red Plexiglas walls (30 cm height) and were allowed free exploration for 10 min, during which the number of rearings were quantified. Footprint characteristics were measured by means of ink deposited on the paws of mice; the animals were then placed at the entrance of a corridor (60 cm long and 7.5 cm wide) with a floor covered with paper. Dynamic balance was evaluated using the horizontal rod test (Rondi-Reig et al., 1999). The aim of this test was to estimate the mouse's ability to maintain its balance while in motion. The apparatus consisted of a horizontal rod (50 cm long, 5 cm in diameter) covered with sticking plaster providing a good gripping surface. It was located 80 cm above a soft carpet to cushion the possible fall of the animals. Both ends of the beam were limited by white altuglass disk (50 cm in diameter). The mouse was placed on the middle of the rod, its body axis perpendicular to the rod axis. During the test, the time before falling, the distance traveled, and the walking time were recorded. The test ended when the animal fell or after 180 s.

To assess motor coordination, an automated hole-board was used (license #DI01873–01) (Rondi-Reig et al., 2008). It consisted of an experimental box made of transparent altuglass (32 × 32 × 25 cm), with a white altuglass floor board, which has 36 holes (2 cm in diameter, 2 cm deep) arranged in a 6 × 6 grid. The mouse was placed in the middle of the board, and its behavior was recorded during 10 min. The walking time and the frequency of stumbles, a measure of motor coordination, were calculated (Rondi-Reig and Mariani, 2002).

The accelerating rotarod (LE-8200; Bioseb) consists of a horizontal rod (3 cm in diameter), turning on its longitudinal axis. Mice were placed on a 5 cm section of the rod facing in the direction opposite to the direction of the rod rotation, such that the animal had to walk forward to avoid a fall. The training phase consisted of walking on the rod turning at a constant speed of 4 rotations per minute (rpm) for successive 30 s trials. When mice successfully walked on the rotating rod during three consecutive 30 s trials, four trials were conducted in which the speed of the rotation increased gradually from 4 rpm to 40 rpm over 5 min. The animal had to coordinate its walk with the rotation speed. This test requires strength, efficient balance, and motor coordination. Time spent on the rotarod was recorded and averaged for the 4 trials.

The muscular strength of the animal's forepaws was measured using a grip test (Bioseb). The mouse was held by the base of its tail and allowed to firmly grab the grid of the device with its forepaws. The mouse was then pulled gently backwards until it released its grip. The peak force (N) of each trial was considered as the grip strength. Four successive measurements were averaged.

Tissue preparation. For light microscopy, mice were anesthetized with sodium pentobarbital (50 mg/kg i.p.) and perfused through the aorta with 0.12 M phosphate-buffer, pH 7.4, containing 4% paraformaldehyde. The cerebella were removed and weighed, then postfixed for 2 h. Some cerebella were cryoprotected in 20% sucrose, frozen in isopentane, and stored at −80°C until cryostat sectioning. Other fixed cerebella were kept

in phosphate buffer at 4°C until vibratome sectioning. Cryostat sections were stored at −80°C and vibratome sections at 4°C until immunostaining.

For immunostaining, sections were blocked for 1 h in PBS containing 0.25% Triton-X, 0.2% gelatin, 0.1% sodium azide and lysine (0.1 M) before applying overnight primary antibody in PBS containing 0.25% Triton-X, 0.2% gelatin, 0.1% sodium azide. Primary antibodies were as follows: goat anti-FOXP2 (1/500; Abcam); goat anti-RORα (1/500; Santa Cruz Biotechnology); mouse or rabbit anti-calbindin-D28K (Calb1) (both 1/5000; Swant); guinea pig anti-vesicular glutamate transporter 1 (VGLUT1, 1/3000; Millipore); guinea pig anti-vesicular glutamate transporter 2 (VGLUT2; 1/3000 Millipore); and chicken anti-GFP (1/200; Aveslab). After washes in PBS containing 0.25% Triton-X and 2 h incubation with a combination of appropriate species-specific secondary antibodies in PBS containing 0.25% Triton-X, 0.2% gelatin, 0.1% sodium azide, the sections were washed several times in PBS and mounted in mowiol (Calbiochem). All the secondary antibodies were from donkey to allow triple or quadruple immunostainings. We used anti-mouse, anti-rabbit, and anti-goat linked to Alexa-488 (1:400; Invitrogen), anti-mouse, anti-rabbit, and anti-goat linked to aminomethylcoumarine (1/50), anti-rabbit and anti-goat linked to Cy3 (indocarbocyanine, 1/500), anti-guinea-pig linked to Cy3 (1/200), anti-mouse, anti-rabbit, and anti-goat linked to Cy5 (indodicarbocyanine, 1/200), and anti-chicken linked to FITC (1/200, Jackson ImmunoResearch Laboratories).

For electron microscopy, three 2-month-old mutant (*Pcp2*::Cre$^{+/-}$;*Rora*$^{fl/fl}$) and three littermate control (*Pcp2*::Cre$^{-/-}$;*Rora*$^{fl/fl}$) male mice were anesthetized with sodium pentobarbital (50 mg/kg i.p.) and perfused with 400 ml of a freshly prepared solution of 2% paraformaldehyde and 2% glutaraldehyde in 0.12 M phosphate buffer, pH 7.3, for 20 min at room temperature. After 1 h at 4°C, the cerebella were carefully dissected out and left in the same fixative 4 h at 4°C. Vermal slices 200 μm thick were cut in the parasagittal plane. The lobule 3 of vermal sections were transferred into a solution containing 2% osmium for 2 h at 4°C. After washes, they were stained "*en bloc*" with a solution containing 2% uranyl acetate for 1 h at 4°C. After washes, samples were dehydrated in graded ethanol followed by acetone and incubated in 50% acetone-50% Araldite for 1 h, followed by 10% acetone-90% Araldite for 2 h. They were then incubated in Araldite for 2 h, before being embedded. Ultrathin (70 nm) sections were cut using an EM UC6 (Leica Microsystems) and collected on 400 mesh copper grids. The sections were stained by incubation with 5% uranyl acetate in 70% methanol for 5 min and then with lead citrate (0.08 M lead nitrate, 0.12 M sodium citrate in CO_2-free dH_2O) for 5 min. The sections were observed with a Philips TECNAI 12 (FEI).

Analysis of RORα expression and PC survival. The time course of RORα expression was analyzed by immunohistochemistry at P10, P14, P21, and P60. Three mutant mice (*Pcp2*::Cre$^{+/-}$;*Rora*$^{fl/fl}$) and their control littermates (*Pcp2*::Cre$^{-/-}$;*Rora*$^{fl/fl}$) were used for each time point. Cerebella were cut on a cryostat into six series of 16-μm-thick sagittal sections. One series was stained with rabbit anti-Calb1 (to label the PCs), guinea pig anti-VGLUT2, and goat anti-RORα antibodies. Another series was stained with goat anti-FOXP2. All the images were acquired using a nanozoomer (Hamamatsu Nanozoomer Digital Pathology, 2.0 HT, its fluorescence unit option, L11600-05, and the NanoZoomer's 3-CCD TDI camera, Hamamatsu Photonics; Cellular Imaging Facility of the Institut de la Vision, Paris) and analyzed with a 20× objective. The numbers of RORα-positive and FOXP2-positive PCs were counted in the anterior lobe (lobules I-V), the posterior lobe (lobules VI-IX), and the lobule X. The means were calculated for each animal, and then the percentage of RORα-positive PCs in mutant animals was normalized to the number of RORα-positive PCs in control animals. PC survival was evaluated by calculating the percentage of FOXP2-positive mutant PCs normalized to the number of FOXP2-positive PCs in the control animals.

Fluorescence quantification of FOXP2 PCs. As PC numbers were obtained by counting FOXP2-positive PC nuclei, we verified that deletion of *rora* did not reduce PC expression of FOXP2 and potentially confound our quantitative analysis. At 2 months, the mean fluorescence signal intensity of FOXP2 immunolabeling was measured in single PCs. We performed the experiment using three different mice per genotype, and for each of them we analyzed at least 30 PCs, in lobule III, from three vermal sections. Pictures were captured at 40× magnification with an exposure time of 500 ms. The mean fluorescence intensity per pixel was measured on FOXP2-positive PC nuclei using MetaMorph.

Analysis of VGLUT2 innervation on the PCs during development. The sections stained with Calb1, VGLUT2, and RORα were also used to measure the height of molecular layer and VGLUT2 terminal distribution in lobule III. Photomicrographs of lobule III from three vermal sections were taken with a 40× objective (DMR microscope, Leica). On these pictures, the thickness of the molecular layer in lobule III was measured at every fifth PC. In parallel, on every fifth PC from three sections of the vermis, we also performed a semiquantification by classifying the somatodendritic distribution of the VGLUT2 puncta on the PC: (1) present only on the soma, (2) present on both the soma and the dendritic tree (soma and dendrites), or (3) present only on the dendritic tree and absent from the soma of the PCs (dendrites only). The distribution among the three different groups was calculated.

Analysis of VGLUT1 and VGLUT2 distribution in the adult mutant mouse. Six series of 50-μm-thick cerebellar vibratome sections from 2-month-old mice, three controls (*Pcp2*::Cre$^{-/-}$;*Rora*$^{fl/fl}$), and three mutants (*Pcp2*::Cre$^{+/-}$;*Rora*$^{fl/fl}$) were analyzed. Sections were stained with anti-Calb1, anti-VGLUT1, or anti-VGLUT2, and anti-RORα. Images of lobule III in the vermis were taken with a Leica SP5 confocal microscope. The 16-bit confocal images were acquired with a 63× objective, a frame size of 1024 × 1024 pixels, and a scan speed of 700 Hz (lines scanned/s), 2-line averaging, and 4-zoom mode. Three regions were analyzed in the lobule III, and three vermis sections were analyzed per animal. The density of VGLUT1 or VGLUT2 immunostaining was measured using MetaMorph 5.0 image analysis system (Universal Imaging). For VGLUT1 immunostaining, the density was measured within a rectangle (730 μm^2) located on the middle part of the molecular layer. For VGLUT2, the density was measured in four different areas. The area termed "PC soma" is a 400 μm^2 circle centered on a PC soma. The area termed "PC stem dendrite" is a 515 μm^2 rectangle containing a PC's stem dendrite. The "middle part of molecular layer" is a 730 μm^2 rectangle positioned two-thirds up the molecular layer. The "superficial part of molecular layer" is a 730 μm^2 rectangle located at the most superficial third of the molecular layer. For appropriate comparison, all the density measures were normalized to 100 μm^2. The absence of RORα immunostaining allows confirmation that the PCs were deleted for *rora*.

Analysis of axon torpedoes. One easily identified morphological change was selected to study the PC axons: the torpedoes (Dusart and Sotelo, 1994). Torpedoes are axonal varicosities in the granular layer with diameters >7 μm. On Calb1-immunostained lobule III, vermal sections from 2-month-old animals (three controls *Pcp2*::Cre$^{-/-}$;*Rora*$^{fl/fl}$ and three mutants *Pcp2*::Cre$^{+/-}$;*Rora*$^{fl/fl}$), we counted the number of torpedoes on at least 100 PCs with clearly visible axons.

Electron microscopic quantification of PF synapses. To count the number of PF synaptic profiles, photomicrographs were taken on one ultrathin section from each of three control and three *rora*-depleted mice. Photomicrographs of 7.74 μm^2 were taken at 20,500-fold magnification every two fields in one square of the 400 mesh grid, located just above the PC layer in the middle of lobule III. Synaptic profiles were then counted in a total of 308 photomicrographs (153 from control and 155 from *rora*-depleted mice). Synaptic profiles crossing two sides of a picture were excluded, whereas those intersecting the two other sides were included. PF synaptic profiles were identified as presynaptic varicosities containing at least three synaptic vesicles and facing a postsynaptic density, and were easily differentiated from CF profiles that contain a higher density of synaptic vesicles in a darker matrix (Palay and Chan-Palay, 1974). The length of postsynaptic densities was measured using ImageJ software (Rasband, 2008).

Anterograde tracer labeling. After behavioral testing, eight mutant (*Pcp2*::Cre$^{+/-}$;*Rora*$^{fl/fl}$) and three control (*Pcp2*::Cre$^{-/-}$;*Rora*$^{fl/fl}$) mice received an injection of anterograde tracer into the inferior olive, as previously described (Sugihara et al., 2003; Dixon and Sherrard, 2006).

Using the obex as a landmark, a micropipette (tip diameter <40 μm) was inserted at 50° from the vertical to a depth determined from a weight–depth curve (Sherrard et al., 1986). The anterograde tracer,

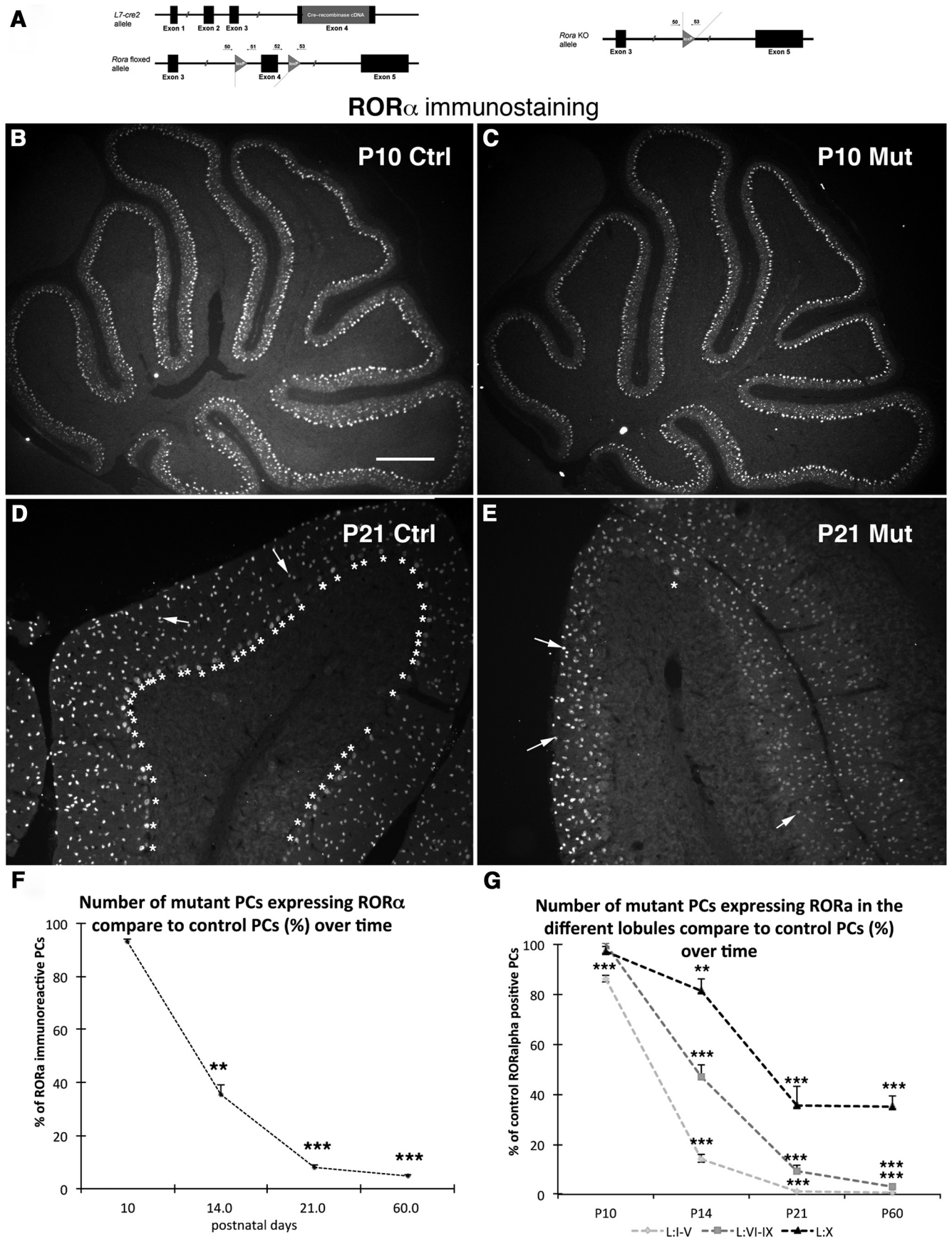

Figure 1. Loss of RORα in mutant Purkinje cells. ***A***, Strategy for the generation of conditional *rora* knock-out mice. The Cre-deleter line (B6.129-Tg(Pcp2::Cre)2Mpin) expresses a *cre* gene inserted into exon 4 of the Pcp2/L7. LoxP sites were introduced flanking exon 4 of the *rora* gene. These floxed mice were bred to the Cre-deleter to generate null alleles. ***B–E***, Photomicrographs of parasagittal cerebellar sections (***B***,***C***) and of lobule III (***D***,***E***) immunostained to reveal RORα from *Pcp2*::Cre$^{-/-}$;*Rora*$^{fl/fl}$ (Ctrl, ***B***,***D***) and *Pcp2*::Cre$^{+/-}$;*Rora*$^{fl/fl}$ (Mut, ***C***,***E***) mice at (*Figure legend continues.*)

lysine fixable dextran-fluorescein solution (4% in distilled water; Fluoroemerald, D-1820 10,000 molecular weight; Invitrogen), was injected into the right inferior olive. In each mouse, there was a single injection of 40 nl placed either medially or mid-laterally in the caudal or mid-rostral region of the inferior olive. The wound was cleaned, the muscles returned to their natural position, the skin sutured, and the animals maintained in a warm box until fully recovered. At 72 h after tracer injections, animals were perfused as described above (tissue preparation). The brainstem and cerebellum were removed, and the inferior olive and cerebellum were cut on a vibratome. The 30 μm sections were taken; the brainstem was always cut coronally and the cerebellum either coronally or parasagittally. Vibratome sections were immunostained for Calb1, RORα, and VGLUT2. Sections were analyzed with a Nikon E800 microscope, and the location of olivary injections and CF terminals was mapped onto outlines of the inferior olive and cerebellar cortex as previously described (Dixon and Sherrard, 2006). The distribution of labeled CF terminals was compared with the areas of labeling, which would be anticipated from the location of the olivary injection according to known olivocerebellar topography (Sugihara and Shinoda, 2004). Images were taken with a Confocal Laser Scanning Microscope (SP5, Leica).

Electrophysiological and morphological analysis. Mice with the genotype *Pcp2*::Cre$^{-/-}$;YFP*stop*$^{fl/fl}$;*Rora*$^{fl/fl}$ were used as controls; these were compared with *Pcp2*::Cre$^{+/-}$;YFP*stop*$^{fl/fl}$;*Rora*$^{fl/fl}$ mutant mice, which lack RORα and express YFP. Fluorescent PCs were considered to be mutant for the purposes of electrophysiological recording.

Mice were deeply anesthetized with inhaled isoflurane and decapitated. Cerebellar slices (250 μm) were prepared and whole-cell patch-clamp recordings from fluorescent PCs performed as previously described (Letellier et al., 2007). Extracellular medium contained (in mM) as follows: 125 NaCl, 2.5 KCl, 1.25 NaH_2PO_4, 1 $MgCl_2$, 2 $CaCl_2$, 26 $NaHCO_3$, 25 D-glucose, saturated with 95% O_2/5% CO_2. Picrotoxin (100 μM) was added to the extracellular recording solution to block inhibitory currents. Patch pipettes were filled with a solution containing the following (in mM): 120 CsD-gluconate, 13 biocytin, 10 HEPES, 10 BAPTA, 3 TEACl, 2 Na2ATP, 2 MgATP, 0.2 NaGTP, pH 7.3, 290–300 mOsm. Recordings were performed using an upright microscope (BX50WI, Olympus) at 20°C. EPSCs resulting from activation of PF-EPSCs or CF-EPSCs were elicited by stimulation with a saline-filled glass pipette in the area surrounding the PC. CF-EPSCs were distinguished from PF-EPSCs by their all-or-none character and by the demonstration of paired-pulse depression (Konnerth et al., 1990). For PCs in which CF-EPSCs were successfully recorded at −80 mV, we subsequently depolarized the PC to −20 mV to avoid voltage-clamp escape of the CF current.

To determine the number of CFs innervating a PC, we counted the number of discrete CF-EPSC steps that appeared when the stimulation intensity was gradually increased and/or when the position of the stimulation electrode was changed.

Synaptic currents were further analyzed using Igor Pro (Wavemetrics) and the NeuroMatic program developed by Jason Rothman (University College London). Amplitudes and rise times for the CF-EPSCs were measured. Several parameters were also evaluated for PF-EPSCs recorded from control and mutant PCs, including the increase in PF-EPSC amplitude with increased stimulus intensity (input–output relationship), and short-term paired-pulse facilitation.

After electrophysiological recordings, slices were fixed in 4% paraformaldehyde in PB 0.1 M and processed for immunohistochemistry. Slices were incubated with streptavidin-Cy3 (1:800, Sigma) for 4 h, and then with anti-RORα overnight to further confirm that the recorded PCs, filled with biocytin, lacked RORα.

Analysis of PC dendritic trees and spines: image acquisition and morphological analysis. The biocytin-filled PCs from the electrophysiological study were used for morphological analysis. Image stacks were obtained with a Confocal Laser Scanning Microscope (SP5, Leica) equipped with a 1.4 NA objective (oil-immersion, 63×, Leica) and with the pinhole aperture set to 1 Airy unit. Images coded in 16 bits depth were acquired in the 570–620 nm emission range and 2 images were taken and averaged for each *z*-step. For whole neuron observation, the pixel size was 240 nm and *z*-step of 1 μm was used. Images stacks were deconvolved using a Maximum Likelihood Estimation algorithm performed with Huygens 3.6 software (Scientific Volume Imaging) with 50 iterations using theoretical PSF. For dendritic spine analysis, the pixel size was set to 60 nm and *z*-step to 0.2 μm. The images were deconvolved with 100 iterations using an experimental PSF, obtained from images of 170 nm diameter fluorescent latex beads (PS-Speck, Invitrogen) (Heck et al., 2012).

For analysis of PC morphology, a 3D model of the dendritic tree was reconstructed using Neuronstudio (version 9.92; Rodriguez et al., 2008) (http://research.mssm.edu/cnic/tools.html) and saved in swc file format. First, the ImageJ plugin tubeness (σ value of 0.8; http://rsb.info.nih.gov/ij/index.html) was applied to the image stack to reinforce tubular structures (i.e., dendrites), and the tree was semiautomatically reconstructed with Neuronstudio; then the 3D model obtained was refined on the original image stack. Dendrite branches were labeled according to Strahler order with Neuronstudio. Order 1 corresponds to terminal branches, and the order number increases toward the soma. Quantitative morphological parameters of the whole neuron were extracted using Lmeasure software (Scorcioni et al., 2008) (http://cng.gmu.edu:8080/Lm/). Sholl analysis was performed with the plugin Simple Neurite Tracer in Fiji program (http://pacific.mpi-cbg.de). For dendritic spine analysis, segments from the upper part of the dendrites were reconstructed so a total of 150–200 μm dendrite length per neuron was analyzed. Automated spine detection followed by manual correction was performed using Neuronstudio. Spine density is defined as the number of spines for 10 μm of dendrite length.

Recombinant lentiviral vectors and production. Recombinant lentiviral vectors expressing Cre or GFP under the control of the CMV promoter were used to prepare stocks of LV-CMV-Cre and LV-CMV-GFP viral particles as previously described (Zennou et al., 2001). Briefly, HEK 293T cells were transiently cotransfected with the p8.91 encapsidation plasmid (Zufferey et al., 1997), the pHCMV-G (vesicular stomatitis virus pseudotype) envelope plasmid, and the pFlap recombinant vectors. The supernatants were collected 48 h after transfection, treated with DNaseI (Roche Diagnostics), and filtered before ultracentrifugation. The viral pellet was then resuspended in PBS, aliquoted, and stored at −80°C until use. The amount of p24 capsid protein was determined by the HIV-1 p24 ELISA antigen assay (Beckman Coulter). Virus from different productions averaged 175 ng/μl of p24 antigen.

Intracerebellar injections of Cre-expressing lentiviral vector into mature Rora$^{fl/fl}$ *mice and analysis of VGLUT2 distribution.* Two-month-old *Rora*$^{fl/fl}$ or YFP*stop*$^{fl/fl}$;*rora*$^{fl/fl}$ male mice were anesthetized by intraperitoneal injection with ketamine (146 mg/kg) and xylazine (7.4 mg/kg) and placed on a Kopf stereotaxic apparatus (Harvard Apparatus). One injection (2 μl, over 8 min) per animal of either LV-CMV-Cre or LV-CMV-GFP was performed on the midline at the suture between the parietal and the occipital bones, and 0.5 mm from pial surface to target lobule VI of the vermis. Two to 4 weeks after the viral injection ($N = 7$ for LV-CMV-Cre, $N = 3$ for LV-CMV-GFP) or 6 weeks ($N = 6$ for LV-CMV-Cre, $N = 5$ for LV-CMV-GFP), the mice were anesthetized and perfused as described above. Sagittal cerebellar vibratome sections (30 μm) were immunostained with Calb1, RORα, GFP, and VGLUT2. Transduced PCs were identified by the presence of both CaBP and GFP immunostaining, and the absence of RORα immunostaining was systematically verified.

←

(*Figure legend continued.*) postnatal day 10 (P10, ***B***,***C***) and P21 (***D***,***E***). Asterisks indicate RORα-immunoreactive Purkinje cells. The interneurons of the molecular layer (arrows) are still RORα-immunoreactive in P21 mutant (***E***). Scale bars: (in ***B***) ***B***, ***C***, 340 μm; ***D***, ***E***, 120 μm. ***F***, ***G***, Number of mutant PCs expressing RORα in different lobules. The mutant values are expressed as a percentage of their respective control values. Percentage of RORα-immunoreactive Purkinje cells in the vermis (***F***) and in the different lobes of the vermis (lobules I-V, lobules VI-IX, and lobule X; ***G***) over time. $N = 3$ mutants and 3 controls at the different ages: P10, P14, P21, and 2 months. Error bars indicate SEM. ***F***, Two-way ANOVA was applied to analyze the effects of genotype ($F_{(1,19)} = 52.63$, $p < 0.0001$) and age ($F_{(3,19)} = 8.34$, $p = 0.001$), followed by a PLSD Fisher *post hoc* analysis. ***G***, Three-way ANOVA was applied to analyze the effects of genotype ($F_{(1,210)} = 6604.17$, $p < 0.0001$), age ($F_{(3,210)} = 729.43$, $p < 0.0001$), and lobules ($F_{(2,210)} = 3198.44$, $p < 0.0001$) followed by a PLSD Fisher *post hoc* analysis to compare control and mutant values at the different ages and the different lobules: $^{**}p < 0.01$; $^{***}p < 0.001$.

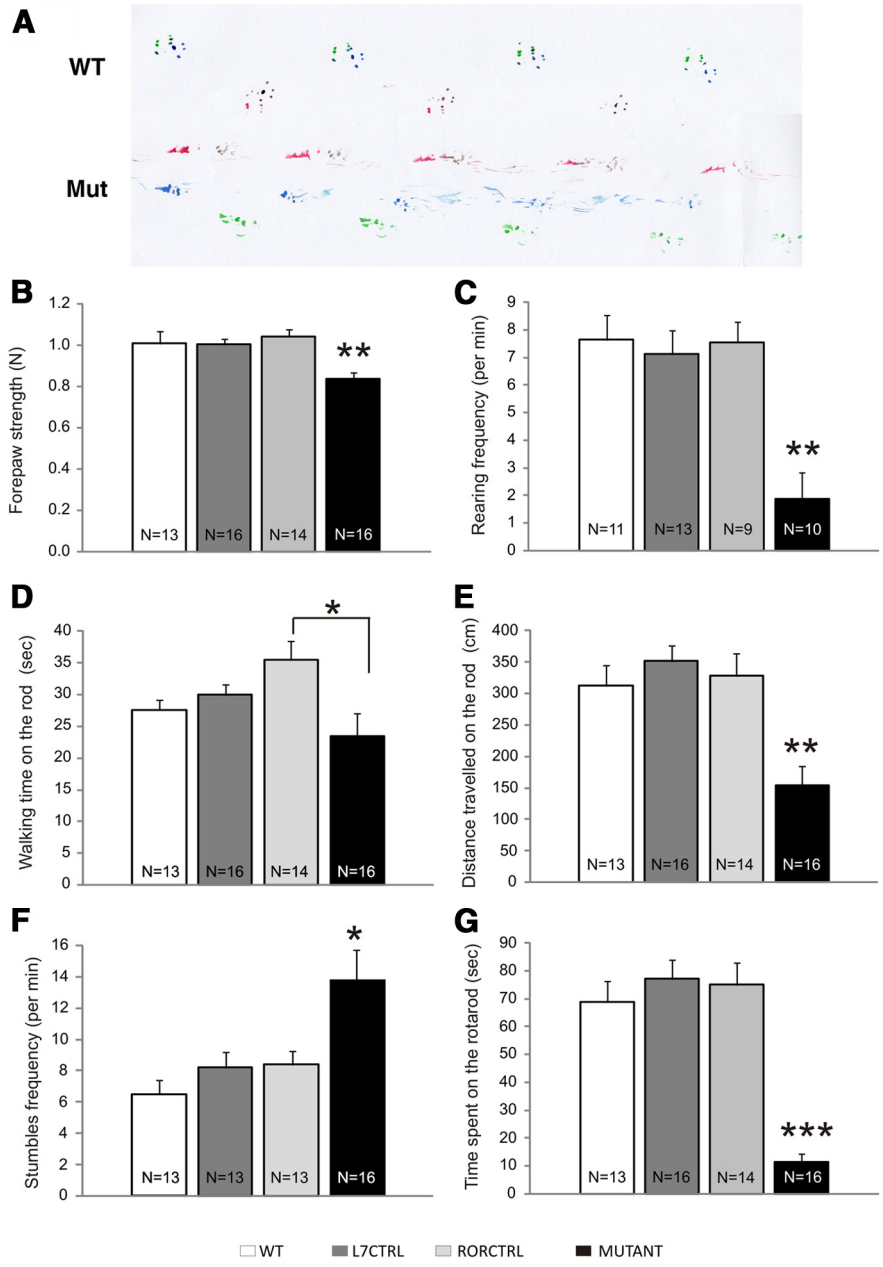

Figure 2. Loss of RORα in Purkinje cells strongly impaired sensorimotor abilities. Different sensorimotor tasks assessed in *Pcp2*::Cre$^{+/-}$;*Rora*$^{fl/fl}$ (Mutant) and the three types of control: *Pcp2*::Cre$^{-/-}$;*Rora*$^{+/+}$ (wild-type control; WT), *Pcp2*::Cre$^{+/-}$;*Rora*$^{+/+}$ (L7Cre control, L7CTRL), and *Pcp2*::Cre$^{-/-}$;*Rora*$^{fl/fl}$ (floxed *Rora* control, RORCTRL). ***A***, Examples of footprint traces in a WT and a mutant mouse. ***B–G***, Analyses of motor performances revealed that the absence of RORα affected muscular strength (***B***), rearing frequency (***C***), dynamic balance (***D***,***E***), and motor coordination (***F***,***G***). Error bars indicate SEM. *N* values are indicated in the bars for each experiment. One-way ANOVA was applied to test the effect of genotype for muscular strength ($F_{(3,55)} = 9.7, p < 0.0001$), rearing frequency ($F_{(3,39)} = 9.4, p < 0.0001$), walking time on the rod ($F_{(3,55)} = 3.67, p < 0.05$), distance traveled on the rod ($F_{(3,55)} = 9.4, p < 0.0001$), the hole-board task ($F_{(3,51)} = 6.2, p < 0.005$), and the time spent on the accelerating rotarod ($F_{(3,55)} = 25.1, p < 0.0001$) followed by Scheffé's *post hoc* analysis. Significant differences between mutant and all control groups, except for ***D***, were as follows: *$p < 0.05$; **$p < 0.005$; ***$p < 0.0001$.

z-stack confocal images (acquired as described above) of the soma and the stem dendrite of these transduced PCs were obtained with Z step of 1 μm. Using ImageJ software, the number of VGLUT2 puncta directly apposed on the soma or on the stem dendrite (first 20 μm) were counted through the stack of images. For the soma, we assigned PCs to three groups: PCs with (1) 0–2, (2) 3–6, and (3) >6 VGLUT2 puncta on their soma. For the stem dendrite, we assigned PCs to four groups as follows: PCs with (1) 0–5, (2) 6–10, (3) 11–15, and (4) >16 VGLUT2 puncta on the first 20 μm of dendritic shaft. The distribution in the different groups of the PCs transduced with LV-CMV-GFP (2–6 weeks), LV-CMV-Cre (2–4 weeks), and LV-CMV-Cre (6 weeks) was calculated.

Statistical analysis. All variables were initially analyzed with the Shapiro–Wilk test to determine whether the data varies significantly from the pattern expected if the data were drawn from a population with a normal distribution. Furthermore, the Levene test was performed to probe the homogeneity of variances across groups. Variables that failed the Shapiro–Wilk or the Levene test were analyzed with nonparametric statistics using Mann–Whitney rank sum tests for comparing two groups. Variables that passed the normality test were analyzed by means of ANOVA followed by a *post hoc* tests (PLSD Fisher, Scheffé, or Dunnett) analysis for multiple comparisons or by Student's *t* test for comparing two groups. Categorical variables were compared using the Fisher's exact test. A *p* value of < 0.05 was used as a cutoff for statistical significance. Data are presented as mean ± SEM. The statistical tests are described in each figure legend.

Results

Time course of the loss of RORα expression in *Pcp2*::Cre$^{+/-}$;*Rora*$^{fl/fl}$ PCs

To deplete RORα specifically from PCs, mice with a floxed *rora* gene were crossed with mice expressing Cre recombinase under control of the PC-specific *Pcp2* gene promoter to obtain control (*Pcp2*::Cre$^{-/-}$; *Rora*$^{fl/fl}$) mice in which RORα is expressed, and mutant (*Pcp2*::Cre$^{+/-}$;*Rora*$^{fl/fl}$) mice in which *rora* has been deleted from the PCs (Fig. 1*A*).

In control mice, RORα was detected immunohistochemically in PCs and molecular layer interneurons at all ages tested as previously described (Fig. 1*B*,*D*) (Ino, 2004). By contrast, in mutant mice, RORα immunoreactivity was present in PCs at P10 (Fig. 1*C*), but almost entirely absent at P21 (Fig. 1*E*), whereas the molecular layer interneurons continued to express RORα (Fig. 1*E*), confirming the specificity of the deletion.

To determine the time course of RORα deletion, we quantified the number of RORα-immunoreactive PCs in the vermis of control and mutant mice. In mutants at P10, 93% of PCs expressed RORα protein. The percentage of these RORα-immunoreactive PCs decreased rapidly between P10 and P21, falling to only 5% at 2 months (Fig. 1*F*). The loss of RORα expression was not homogeneous throughout the cerebellar cortex (Fig. 1*G*), occurring earlier in the anterior lobe (lobules I-V) than in the posterior lobe (lobules VI-IX), and *rora* deletion in lobule X was much reduced compared with other lobules (Fig. 1*G*).

These data show that PC-specific RORα depletion occurs in this model during a relatively late stage of PC development, mainly between P10 and P21. We thus used this mutant mouse

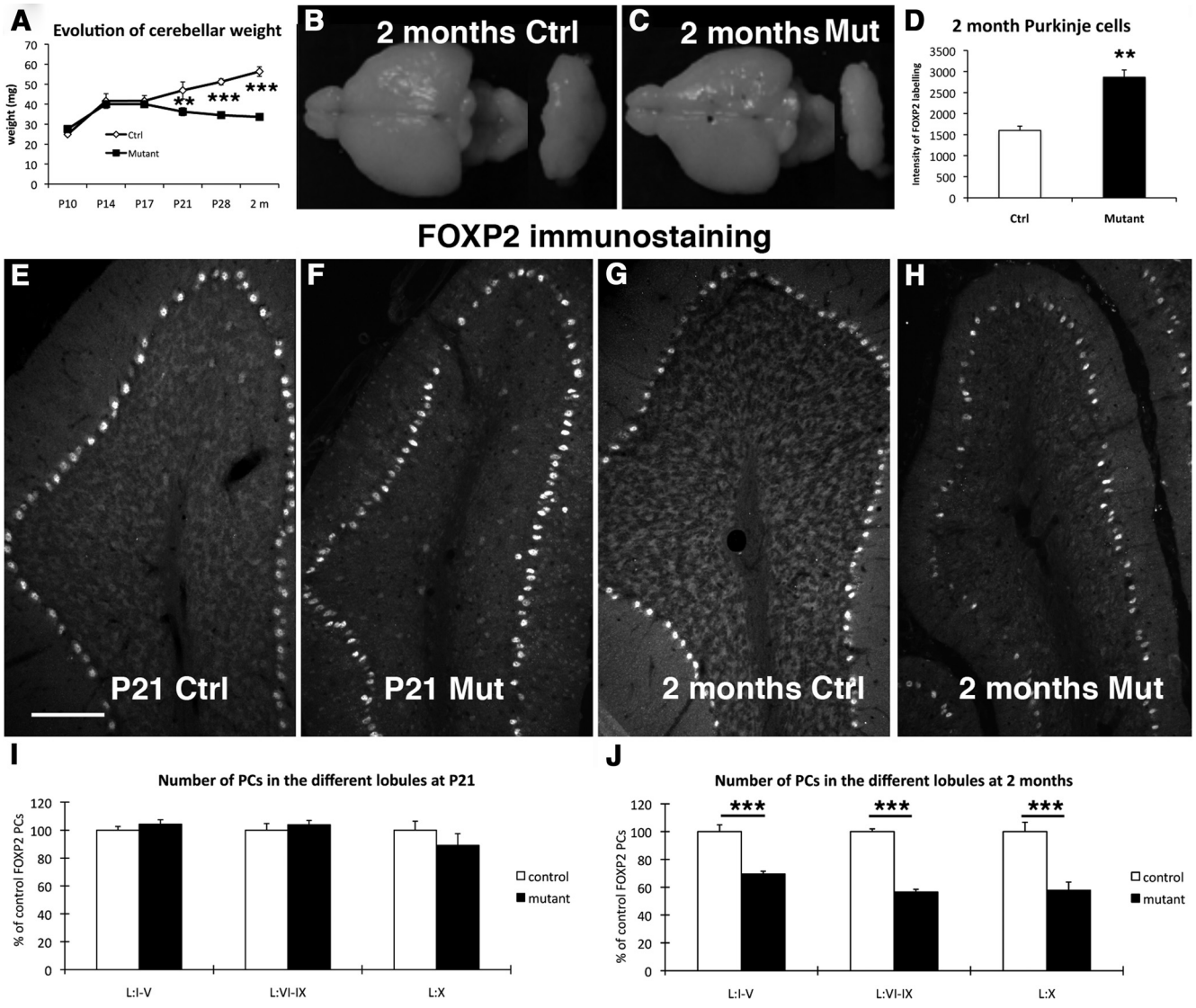

Figure 3. Loss of RORα in Purkinje cells leads to cerebellar atrophy and Purkinje cell loss. ***A***, Changes in cerebellar weight during late development; two-way ANOVA was applied to analyze the effects of genotype ($F_{(1,33)} = 35.80$, $p < 0.0001$) and age ($F_{(4,33)} = 11.52$, $p = 0.001$), followed by a PLSD Fisher *post hoc* analysis to compare control and mutant at each age: $^{**}p < 0.01$; $^{***}p < 0.001$. ***B***, ***C***, Images of *Pcp2*::Cre$^{-/-}$;*Rora*$^{fl/fl}$ (Ctrl, ***B***) and *Pcp2*::Cre$^{+/-}$;*Rora*$^{fl/fl}$ (Mut, ***C***) brains and their cerebella at 2 months showed that *rora* deletion changes only the cerebellar size. ***D***, Graphic representation of the mean fluorescence intensity of FOXP2 immunostaining in Purkinje cell nuclei. Error bars indicate SEM. $^{**}p < 0.01$ (Student's *t* test). ***E–H***, Photomicrographs of FOXP2-immunostained lobule III in vermis parasagittal cerebellar sections from *Pcp2*::Cre$^{-/-}$;*Rora*$^{fl/fl}$ (Ctrl, ***E***,***G***), and *Pcp2*::Cre$^{+/-}$;*Rora*$^{fl/fl}$ (Mut, ***F***,***H***) at P21 (***E***,***F***) or 2-month-old (***G***,***H***). Scale bar, 120 μm. ***I***, ***J***, Percentage of mutant FOXP2-immunoreactive PC in the lobules I-IV, lobules VI-IX, and lobule X of the vermis at P21 (***I***) and 2 months (***J***). Error bars indicate SEM. ***I***, Two-way ANOVA was applied to analyze the effects of genotype and lobules; no difference was detected between the two genotypes. ***J***, Two-way ANOVA was applied to analyze the effects of genotype ($F_{(1,12)} = 373.12$, $p < 0.0001$) and lobules ($F_{(2,12)} = 455.37$, $p < 0.0001$) followed by a PLSD Fisher *post hoc* analysis: $^{***}p < 0.001$.

(*Pcp2*::Cre$^{+/-}$;*Rora*$^{fl/fl}$) to study the role played by RORα in PCs after their early developmental phases.

Rora deletion in PCs after the first postnatal week impairs motor coordination

Because defects in PC function are generally associated with impaired motor behavior, we tested motor behavior in adult *rora*-deleted mice. The first signs of motor dysfunction were detected 4–5 weeks after birth, with very slight tremors during locomotion. The symptoms became more evident at 7–8 weeks of age, with the development of an ataxic gait. We therefore performed a complete motor behavior study on 2-month-old mice. A footprint assay revealed that the mutant mice had an irregular gait compared with controls, with an abnormally large hindpaw angle relative to the direction of walking, indicating reduced hindlimb motor coordination (Fig. 2*A*). In addition, forepaw muscular strength was also reduced (Fig. 2*B*). Analysis of locomotor activity in the open field revealed that rearing frequency was drastically reduced in the mutant mice compared with the three control groups (described in Materials and Methods; Fig. 2*C*). Dynamic balance was also affected in the mutant mice as revealed by the significant reduction in both walking time (Fig. 2*D*) and distance traveled on the rod (Fig. 2*E*). Finally, motor coordination was also strongly affected by the deletion of *rora* from PCs, with the mutant mice showing significantly more stumbles than controls in the hole-board task (Fig. 2*F*) and impaired performance on the accelerating rotarod (Fig. 2*G*). These data indicate that mice with PC-specific *rora* deletion had a strong impairment of motor abilities, presumably resulting from PC dysfunction and/or loss.

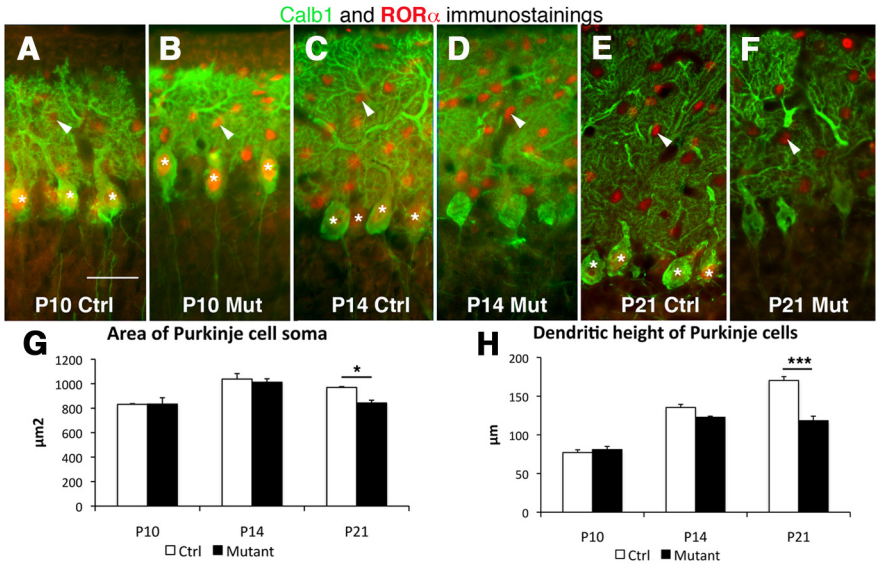

Figure 4. Dendritic tree of mutant Purkinje cells is reduced in height from P21. ***A–F***, Photomicrographs of lobule III from vermis parasagittal cerebellar sections double immunostained for Calb1 (green) and RORα (red) from *Pcp2*::Cre$^{-/-}$;*Rora*$^{fl/fl}$ (Ctrl, ***A***,***C***,***E***) and *Pcp2*::Cre$^{+/-}$;*Rora*$^{fl/fl}$ (Mut, ***B***,***D***,***F***) at P10 (***A***,***B***), P14 (***C***,***D***), and P21 (***E***,***F***). Asterisks label RORα-immunoreactive Purkinje cell nuclei. There is the disappearance of RORα immunostaining in mutant PCs from P14, whereas it is still present in the nucleus of molecular interneurons (arrowheads). Scale bar, 30 μm. ***G***, ***H***, Graphic representations of the surface of PC soma (***G***) and the PC dendritic height (***H***). Error bars indicate SEM. Two-way ANOVA was applied to test the effects of genotype ($F_{(1,12)} = 5.048$, $p < 0.05$); and age ($F_{(2,12)} = 18.55$, $p < 0.001$) for the soma (***G***) and genotype ($F_{(1,12)} = 36.38$, $p < 0.0001$) and age ($F_{(2,12)} = 135.96$, $p < 0.0001$) for dendritic height (***H***), followed by a PLSD Fisher *post hoc* analysis to compare between genotypes: $^{*}p < 0.05$; $^{**}p < 0.01$.

Rora deletion after the first postnatal week reduces the number of PCs in the adult

To evaluate the cause of the motor dysfunction, we first examined the survival of *rora*-deficient PCs. It is known that mutant or transgenic mice that lack functional RORα throughout development have greatly reduced numbers of cerebellar PCs (Dussault et al., 1998; Vogel et al., 2000; Doulazmi et al., 2001). In addition, mice haploinsufficient for *rora* show earlier aging-related PC death (Zanjani et al., 1992; Hadj-Sahraoui et al., 1997; Doulazmi et al., 1999; Janmaat et al., 2011). We thus asked whether deletion of *rora* after the initial period of cerebellar development also affected PC survival.

From P10 to P17, the weight of cerebella from mutant mice was comparable to control littermates at the same age (Fig. 3*A*), but from P21 the cerebellar weight of mutant mice remained stable, whereas that of controls continued to increase (Fig. 3*A–C*). No defects in foliation were observed. When PC nuclei were labeled using FOXP2 immunostaining, no differences were observed between mutant and control cerebella at P21 (Fig. 3*E*,*F*), but there were many gaps in the PC layer of mutants at 2 months (Fig. 3*G*,*H*). To determine whether these gaps were the result of decreased FOXP2 expression in mutant PCs and thus faulty detection, we measured the fluorescent intensity of FOXP2 immunoreactivity in mutant and control PC nuclei. In fact, we actually observed increased intensity of FOXP2 immunoreactivity in mutant PCs compared with controls (Fig. 3*D*). We therefore used FOXP2 immunostaining to determine PC number. The PC counts in the vermis of mutant and control animals were similar at P21 but 30% lower in the mutant at the age of 2 months (Fig. 3*I*). The PC loss was uniform throughout the different lobules (Fig. 3*J*). At P21, although RORα protein was detectable in only 8% of the PCs (Fig. 1*F*), PC number in the mutant mice was similar to that of controls (Fig. 3*I*). In addition, although loss of RORα expression occurred earlier in the anterior lobe (Fig. 1*G*), rates of PC loss were similar in the anterior and posterior lobes (Fig. 3*J*), indicating that PC maturation at the time of *rora* deletion did not affect survival.

PC-specific *rora* deletion after the first postnatal week induces atrophic changes in mature PCs

The motor dysfunction we observed could also be the result of abnormal morphologic maturation of the surviving PCs. RORα is well known to be essential for dendritic development in PCs, and specifically the transition from early transient bipolar dendrites to the later permanent dendritic tree (Boukhtouche et al., 2006b). We evaluated the potential role of *rora* in the later stages of PC morphological maintenance. The quantification of Calb1-immunostained cells revealed no difference either in the size of the PC body (Fig. 4*G*) or the height of the PC dendritic tree (Fig. 4*H*) between P10 mutant and control mice, an age at which most PCs still express RORα (Fig. 4*A*,*B*). The same phenotype was found at P14 (Fig. 4*G*,*H*), an age at which most of the mutant PCs are devoid of RORα (compare Fig. 4*C*,*D*). However, by P21, mutant mice showed smaller PC cell bodies (Fig. 4*E–G*) and a considerable reduction in the height of the PC dendritic tree (Fig. 4*E*,*F*,*H*) associated with a reduction of the height of the molecular layer. Then, we evaluated the axons and dendritic trees of adult mutant RORα-deleted PCs.

An analysis of PC axonal morphology was performed in mutant and control mice at the age of 2 months. Axons in the mutant were not entirely normal, with a higher incidence of torpedoes compared with controls (14% and 0.5%, respectively). These results indicate that some PC axons were modified in the absence of *rora*.

To study dendritic morphology of individual PCs, we analyzed dendritic trees of PCs filled with biocytin. At P15, no differences were detected between control PCs and PCs lacking RORα (Fig. 5*A*), but the effects of the *rora* deletion were obvious at later ages. In 1-month-old animals (Fig. 5*B*), 30% (4 of 14) of the mutant PCs had a tree complexity similar to control, but with a reduced size ("small PCs"), whereas most mutant cells (70%, 10 of 14) had a highly atrophic dendritic tree ("atrophied PCs"). Because these two morphological mutant phenotypes were characterized by different overall shape, they were separated for quantitative 3D analysis (Fig. 5*C–E*). Whereas the height of the dendritic tree and the total dendritic length were highly reduced both in small and atrophied PCs, the width of the dendritic tree was only reduced in the atrophied PCs (Fig. 5*C*). Sholl analysis represents the density of branch points at different distances from the soma. Compared with control PCs, small PCs had similar numbers of branch points, but the tree was shorter, whereas the atrophied PCs had very low dendritric complexity on a very small tree (Fig. 5*D*). Moreover, in agreement with a Sholl analysis, a major reduction in the Strahler orders was observed for atrophied PCs, whereas only one order was lost for the small PCs (Fig. 5*C*). Our results indicate that the atrophy process in these small PCs does not affect all parts of the dendritic complexity equally:

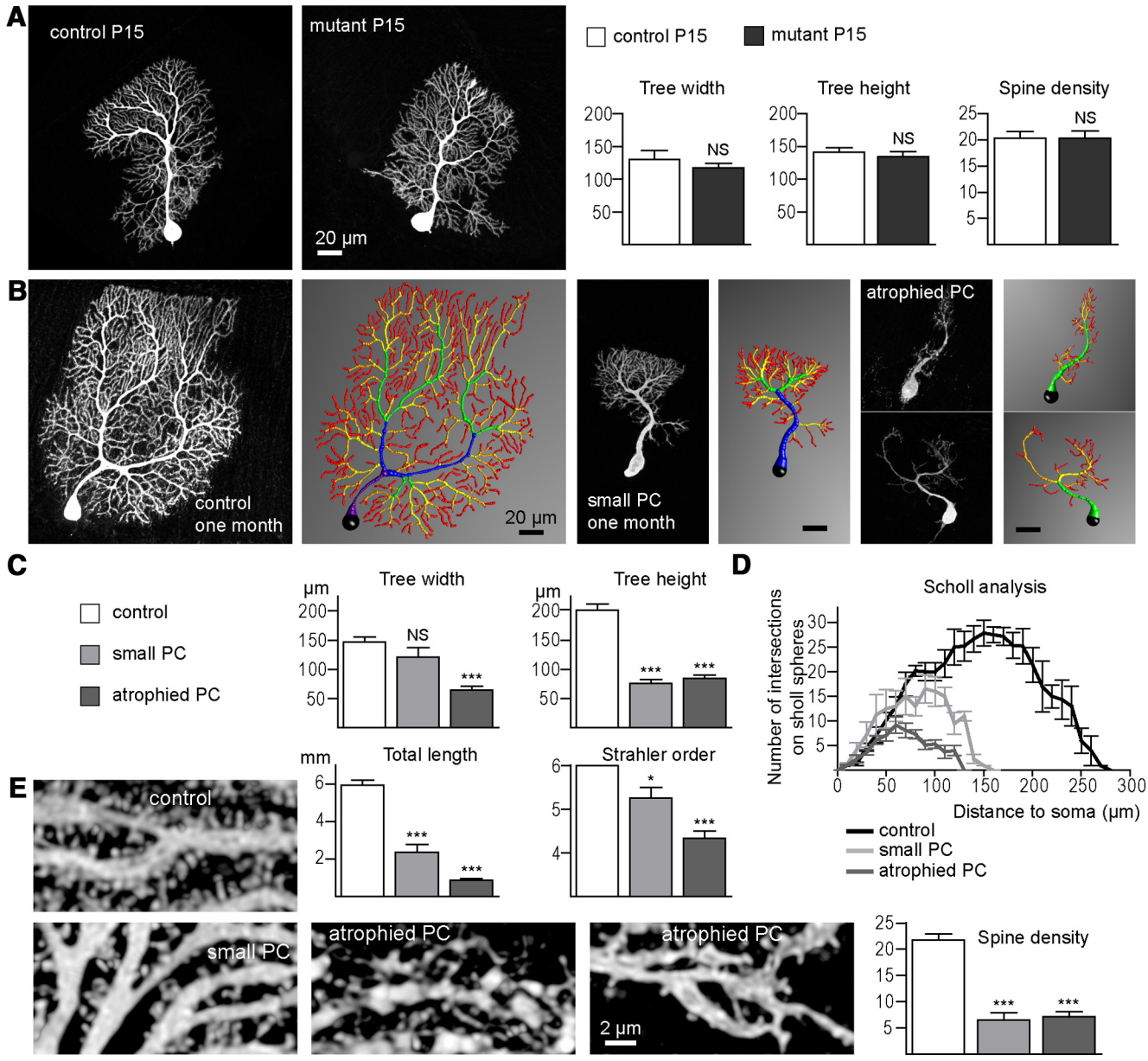

Figure 5. Morphology of mutant Purkinje cells. ***A***, Representative control and mutant Purkinje cells filled with biocytin at P15. Neither tree size nor spine density is affected at this stage, although these PCs lacked RORα. Error bars indicate SEM. No difference was detected (width or height: Student's *t* test; and spine density: Mann–Whitney test). ***B***, Representative control, small, and atrophied Purkinje cells with their respective 3D dendritic tree model in 1-month-old animals. The Strahler orders are color-coded on the models. The small Purkinje phenotype exhibits a particular tree shape that is different from the atrophied cells. ***C***, Reconstruction of dendritic trees allows measurements and analysis of width, height, total dendrite length, and Strahler orders. All measurements are performed in three dimensions on the whole dendritic tree. ***D***, Sholl analysis of control and mutant dendritic trees. A different pattern is observed for the two mutant phenotypes. Small Purkinje cells have similar branch complexity but reduced height compared with control. Atrophied cell trees have small size and major loss of branches. ***E***, Spine densities measured on upper dendrites show a similar decrease for both mutant cell populations compared with control. Scale bar, 20 μm for all Purkinje cell images and 2 μm for all dendritic spine images. Error bars indicate SEM. For statistical analysis, measurements from control neurons were compared with the mutant phenotypes using one-way ANOVA for the following parameters: tree width ($F_{(2,17)} = 24.14, p < 0.0001$), tree height ($F_{(2,17)} = 78.62, p < 0.0001$), total length ($F_{(2,16)} = 143.1, p < 0.0001$), Strahler order ($F_{(2,16)} = 29.67, p < 0.0001$), and spine density ($F_{(2,16)} = 50.83, p < 0.0001$) followed by Dunnett *post hoc* test. NS, Nonsignificant. $^*p < 0.05$. $^{***}p < 0.001$. $N = 6$ control, 4 small, and 10 atrophied PCs.

loss of entire proximal dendritic branches occurred rather than a uniform centripetal dendritic regression.

Finally, the spine density measured in the upper dendritic branches was highly reduced in both small and atrophied mutant PCs (Fig. 5*E*).

It is important to note that the general morphology of the mutant PC dendritic trees appeared more mature at P15 than at 1 month of age. This indicates that the deletion of *rora* in our model does not interfere with early PC development but rather induces the regression of the mature dendritic morphology.

Rora deletion in PCs after the first postnatal week induces a decrease of VGLUT1 terminal density and a redistribution of VGLUT2 terminal density on mature PCs

Because the mutant PC dendritic trees are less elaborate, with fewer branches and distal spines, we asked whether *rora* deletion during the second and third postnatal weeks influences the number and location of their glutamatergic presynaptic partners (i.e., PFs and CFs). PF terminals, identified using anti-VGLUT1 immunohistochemistry, were observed in the molecular layer of both control (Fig. 6*A*) and mutant (Fig. 6*B*) cerebella in

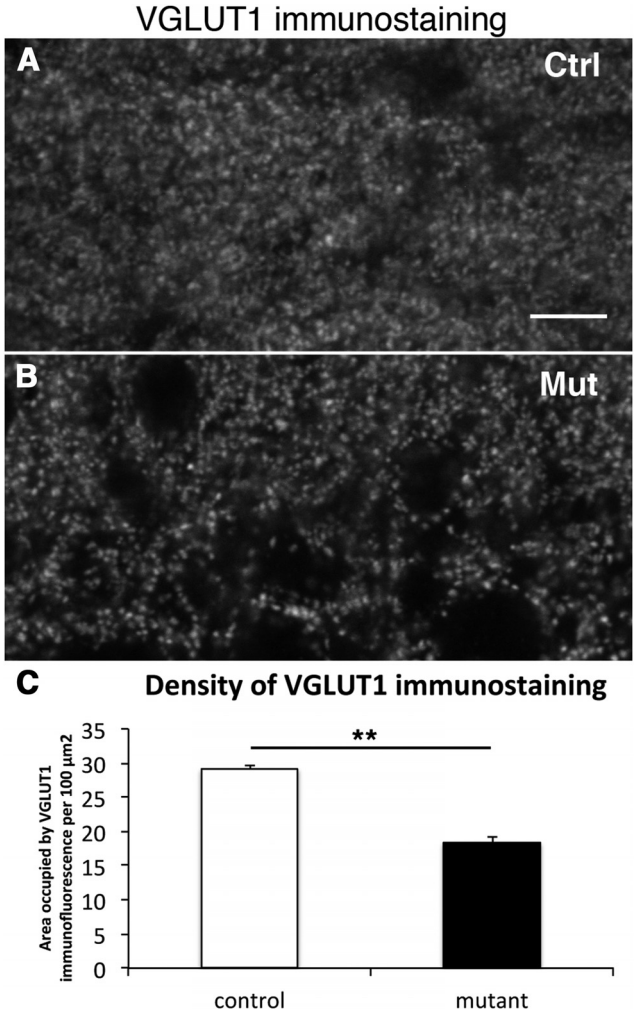

Figure 6. VGLUT1 immunostaining decreases in mutant molecular layer. ***A***, ***B***, Confocal images of vermal lobule III from 2-month-old *Pcp2*::Cre$^{-/-}$;*Rora*$^{fl/fl}$ (Ctrl, ***A***) and *Pcp2*::Cre$^{+/-}$;*Rora*$^{fl/fl}$ (Mut, ***B***) parasagittal cerebellar sections stained for VGLUT1. Scale bar, 7 μm. ***C***, Graphic representation of the density of VGLUT1 immunostaining in the molecular layer: area occupied by VGLUT1 immunofluorescence per 100 μm^2. Error bars indicate SEM. $^{**}p < 0.01$ (Student's *t* test). Three animals were analyzed for each genotype and 9 fields per animal.

2-month-old animals. However, a 40% reduction in the density of VGLUT1 immunostaining was observed in mutants compared with control littermates (Fig. 6*C*).

Using VGLUT2 immunohistochemistry, we then determined the location of CF terminals on control and mutant PCs at 2 months of age. In control mice, VGLUT2 staining appeared as previously described (Miyazaki et al., 2003): rarely around the soma, very little on stem dendrites, and mainly distributed on the other parts of the primary dendritic compartment (Fig. 7*A–C*; i.e., in the middle part of the molecular layer; Fig. 7*G*). In contrast, in the *rora*-deleted mutant mice, VGLUT2-immunopositive puncta were observed around the PC soma and the stem dendrite (Fig. 7*E*,*F*), but seldom on the middle and upper dendrites (Fig. 7*D*; i.e., in the middle and superficial part of the molecular layer; Fig. 7*G*). Densitometric analysis showed that, compared with the controls, the density of VGLUT2 immunoreactivity was 42 times higher on the soma in mutants but was less dense (one-sixth) in the mid-molecular layer (Fig. 7*G*). Moreover, the increased density of VGLUT2-stained terminals on the soma, and stem dendrite was associated with the presence of thorn spines (Fig. 7*F*), such as those seen during the developmental "capuchon" stage of CF development (Ramón y Cajal, 1911; Chédotal and Sotelo, 1992, 1993; Sugihara, 2006).

To determine at what age the altered distribution of VGLUT2-immunopositive puncta began in control and mutant PCs, we quantified the localization of VGLUT2 staining at P10, P14, and P21, determining the relative distribution of VGLUT2 staining on the soma and dendrites. During development, VGLUT2 labels both climbing and PF terminals; however, it is possible to distinguish between the large CF puncta and the diffuse PF labeling (Fig. 8). We categorized three types of distribution of VGLUT2-positive CF puncta on PCs as follows: (1) CF puncta only on the PC soma, (2) CF puncta on both the soma and the dendrites, and (3) CF puncta on the dendrites only.

At P10, large VGLUT2 puncta were seen on the proximal dendrites of both control and mutant PCs (Fig. 8), indicating that normal developmental somatodendritic CF translocation was well underway in both cases. In P14 controls, most puncta were absent from the PC soma and were localized on the dendrites. In the mutant, a considerable proportion of VGLUT2-positive puncta (27%) still contacted both the soma and the dendrite. It is important to note that the percentage of mutant PCs with large VGLUT2 puncta apposed to the dendrites was higher at P14 (72%) than at P21 (54%), indicating that the deletion of *rora* does not simply block CF somatodendritic translocation: the deletion reverses this process and favors the reestablishment of CF innervation on the soma.

Electron microscopy of excitatory synaptic inputs to PCs in 2-month-old mutant mice

At 2 months, electron microscopic observations suggest no ongoing degenerative process in mutant mice. Necrotic debris were seen only rarely, facing normal-looking PF varicosities, or in phagocytic cells along with lipid inclusions. The drastically reduced molecular layer contained large numbers of astrocytic profiles filled with gliofilaments, most likely the result of reactive gliosis after the death of some PCs (Fig. 9*F*). Surviving PCs were atrophic, with smaller somata and dendritic trees than in the controls, as observed in light microscopy. In addition, and as is the case in the staggerer mutant mouse (Sotelo, 1975), the hypolemmal cisterna (Palay and Chan-Palay, 1974) was very poorly developed. However, accumulations of short tubular and vesicular profiles consistent with smooth endoplasmic reticulum, hypolemmal cisterna, were frequently observed in spine-like profiles (Fig. 9*A*) as well as in medium-sized dendrites (Fig. 9*B*). The latter did not resemble the stacks of flattened cisterna reported after a few minutes of anoxia, which correspond to fixation artifacts (Takei et al., 1994).

The most notable characteristic of these dendritic trees was the scarceness of long-necked spines, which are the postsynaptic elements of PF synapses onto PCs. Spiny branchlets were practically absent, although some long filopodial-like processes occasional emerged from smooth medium-sized dendrites (Fig. 9*D*). Axo-spinous synapses on PCs were much less frequent (Fig. 9*A*) in mutants than in controls, and some occasional synapses were established with spines emerging from large proximal branches of PC dendrites (Fig. 9*D*); this is similar to what is seen in PCs that have lost their CF innervation (Sotelo et al., 1975). In the molecular layer, the PF varicosities were often apposed to neuronal perikarya or covering the surface of dendritic segments (Fig. 9*C*,*J*). Furthermore, some of the remaining PC spines and filopodia were contacted by more than one PF (Fig. 9*B*) and could even be shared by a PF and a CF varicosity (Fig. 9*F*). Nevertheless, the density of synaptic profiles established by PF varicosities remained at ~50% of control value (Fig. 9*I*), in ac-

cordance with the results of VGLUT1 immunohistochemistry. This reduction of synaptic profile density was likely the result of a true loss of synapses rather than their shrinkage because there was no difference in the size of postsynaptic densities (Fig. 9*K*). To determine whether the remaining PF synapses were functional, we measured the input–output relationship and the maximum PF-EPSC amplitudes recorded in control and mutant PCs. There were no significant differences in these parameters between the two groups (data not shown), indicating that, although PF synaptic contacts are differently organized on the mutant PCs, they are still functional.

As reported above with light microscopy, the CFs innervating the mutant PCs did not reach the upper half of the thinner molecular layer. They rather showed characteristics of the immature "capuchon" stage (Chédotal and Sotelo, 1992), with CF contacts on the PC cell body. At the ultrastructural level, CF varicosities were easily identified by several morphological parameters (Larramendi and Victor, 1967), including the tight packing of spherical synaptic vesicles, filling almost the entire surface of the varicosity, together with the occurrence of large granulated vesicles and the dense appearance of the axoplasm (Fig. 9*E–H*). Although CF varicosities were not very numerous, they were systematically observed in proximity to the PC perikarya and in the neuropil of the deeper part of the molecular layer, close to the emergence of the stem dendrites, in parallel with ascending collaterals of basket cell axons (Fig. 9*H*) as in control PCs (Chan-Palay and Palay, 1970). They were occasionally apposed to the smooth surface of the PC somata, linked to them through attachment plates, or contacting small somatic protrusions (Fig. 9*G*). In the molecular layer, CF established synaptic contacts with either short thorns emerging form presumptive PC dendrites (Fig. 9*F*), with hypertrophic spines forming pseudo-glomerular arrangements wrapped in several layers of thin astrocytic processes (Fig. 9*E*), or sometimes in close vicinity to spines emerging from primary dendritic stems. Together, these observations showed that PCs did not present signs of ongoing degenerative processes, but they did have an almost-complete loss of dendritic spiny branchlets. The PF and CF innervations were reorganized and mixed, the PFs mainly contacting the remaining spines and the smooth surface of PC dendrites and the CFs contacting the PC soma and stem dendrite.

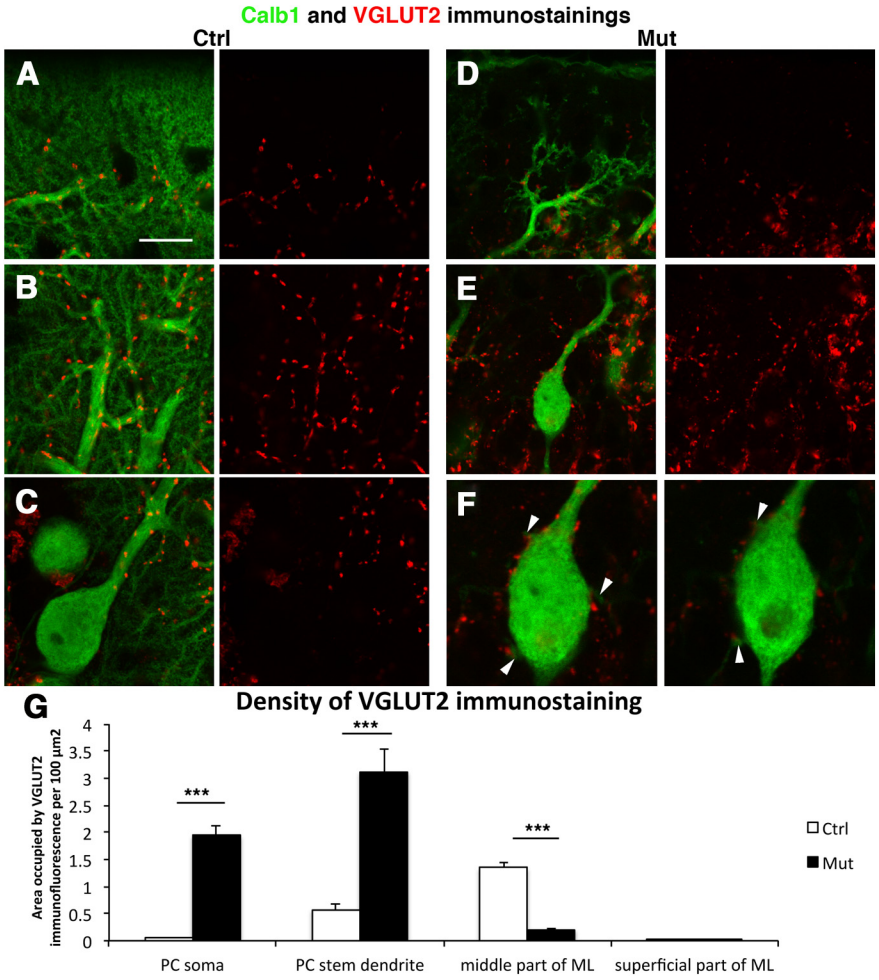

Figure 7. Distribution of VGLUT2 immunostaining is different in mutant compared with control. ***A–F***, Confocal images of vermal lobule III from 2-month-old *Pcp2*::Cre$^{-/-}$;*Rora*$^{fl/fl}$ (Ctrl, ***A–C***) and *Pcp2*::Cre$^{+/-}$;*Rora*$^{fl/fl}$ (Mut, ***D–F***) parasagittal cerebellar sections double stained for Calb1 (green) and VGLUT2 (red). There is the absence of VGLUT2 in the superficial part of the molecular layer both for control and mutant (***A***,***D***), the decrease of VGLUT2 immunostaining in the middle part of the mutant molecular layer (***D***) compared with control (***B***), whereas there is an increase on the mutant soma and stem dendrite (***E***) compared with control (***C***). ***F***, Enlarged from ***E***, representing two serial confocal sections. There is the presence of varicosities on the soma of the Purkinje cells (arrowheads). Scale bars: ***A–E***, 15 μm; ***F***, 7.5 μm. ***G***, Graphic representation of the density of VGLUT2 immunostaining in the molecular layer: area occupied by VGLUT2 immunofluorescence per 100 μm^2 (see Materials and Methods for description). Error bars indicate SEM. Two-way ANOVA was applied to test the effects of genotype ($F_{(1,64)} = 9.55, p < 0.001$) and location ($F_{(3,64)} = 10.97, p = 0.001$) followed by a PLSD Fisher *post hoc* analysis: ***$p < 0.001$. Three animals were analyzed for each genotype and 9 fields per animal.

Rora deletion in PCs after the first postnatal week triggers CF multi-innervation

The developmental elimination of supernumerary CF synapses does not occur in the absence of RORα (Crepel et al., 1980; Mariani and Changeux, 1980). However, it was not clear whether this is strictly a developmental effect or whether late deletion of *rora* later in development would have any effect once mono-innervation is achieved. Is continued RORα expression necessary to maintain this synaptic specificity?

In mutant mice, recombination occurs mainly between P10 and P21 (Fig. 1); thus, RORα is present during the embryonic (E14, Hamilton et al., 1996) and early postnatal period and is then no longer synthesized starting at an age when CF synapse elimination is well underway or nearly complete (Kano and Hashimoto, 2009). Our morphological studies revealed dendritic changes and particularly a reversal of the CF somatodendritic translocation, suggesting functional changes in the CF/PC synapses. We thus evaluated the maturation of CF innervation to PCs in adult mutant mice using both anterograde tract tracing and electrophysiology.

Consistent with the VGLUT2 labeling and ultrastructure described above, in 2-month-old mutants, anterogradely labeled CF terminals showed abnormal structure: specifically, they were

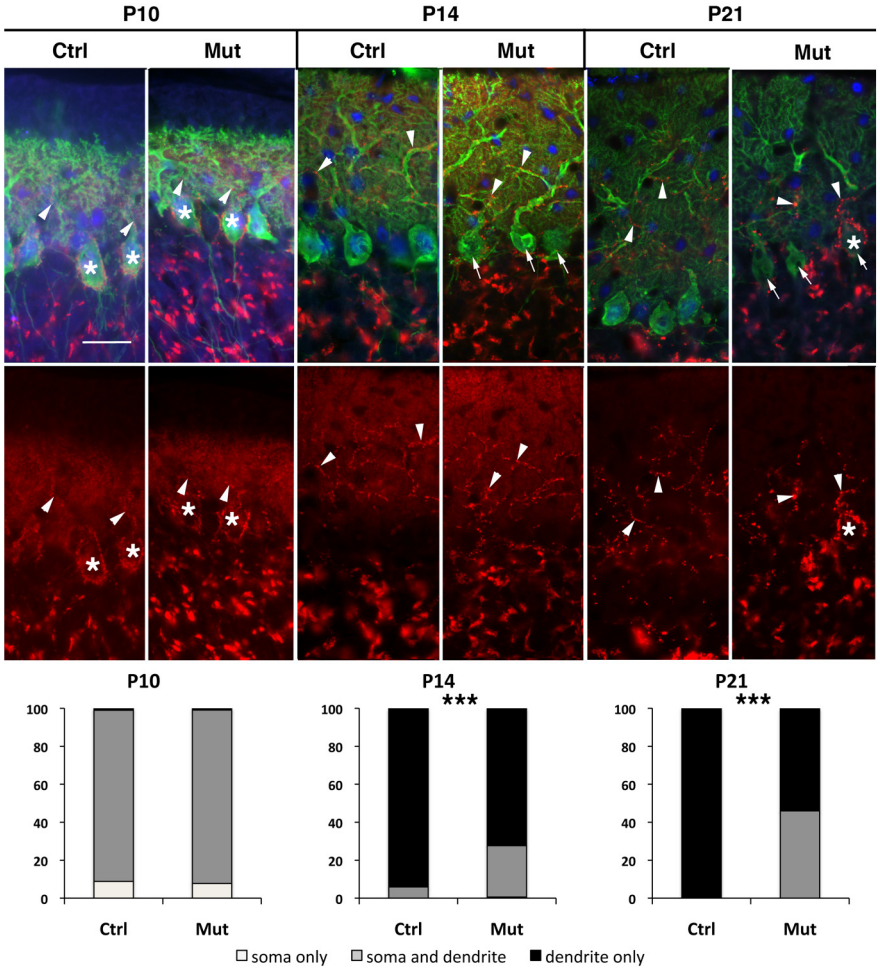

Figure 8. Developmental distribution of VGLUT2 immunostaining. Photomicrographs of lobules III from vermis parasagittal cerebellar sections triple immunostained for Calb1 (green), VGLUT2 (red), and RORα (blue) from *Pcp2*::Cre$^{-/-}$;*Rora*$^{fl/fl}$ (Ctrl) and *Pcp2*::Cre$^{+/-}$;*Rora*$^{fl/fl}$ (Mut) at P10, P14, and P21. *Purkinje cell somata in contact with VGLUT2-immunoreactive puncta. Arrowheads indicate VGLUT2 puncta on Purkinje cell dendrites; arrows indicate PC soma lacking RORα. Scale bar, 30 μm. Graphic representation of the distribution of the VGLUT2 puncta on Purkinje cells at P10, P14, and P21. ***$p < 0.001$ (Fisher's exact test).

shorter and concentrated around the PC soma and lower dendritic branches. Importantly, these adult mutant PCs were contacted by two types of CF terminals: those that were single-labeled only by VGLUT2 and others that were double-labeled by both VGLUT2 and Fluoremald tracer, which is consistent with innervation by at least two separate CF axons (Fig. 10*A*) (Miyazaki and Watanabe, 2011). Electrophysiological recordings demonstrated the degree of CF multi-innervation: of 33 mutant PCs recorded from 5 mutant animals (1-month-old), only 12 were mono-innervated (Fig. 10*B*,*C*). In parallel experiments using control littermates of the mutant animals, we found no multiple CF innervation ($N = 21$ cells, from 3 animals, Fig. 10*C*). These results thus indicate that the loss of RORα expression has a strong effect on the CF innervation state of PCs in these mice.

In some previous reports of mutant mice, a return to multiple CF innervation of PCs in the mature cerebellum has been shown to involve new CFs contacting the most distal part of the dendritic tree (Miyazaki et al., 2010). The EPSCs from these distal-contacting CFs have slow kinetics, with rise times of up to 6 ms in some cases, whereas CFs contacting the normal proximal dendritic compartment have rise times <1 ms (Miyazaki et al., 2010, their Fig. S5). We thus compared the rise times of CF-EPSCs recorded in control and mutant PCs to determine whether the multiple CFs contacting the mutant PCs were in the same dendritic compartment, as suggested by tracing studies and immunohistochemistry. We found no significant differences in rise times of CF-EPSCs between mutant and control PCs: CF-EPSC rise times varied from 0.71 to 1.18 ms in control PCs and 0.53–2.68 ms in mutant PCs (Fig. 10*D*). More importantly, in the multi-innervated mutant PCs, the rise times of CF-EPSCs on the same PC did not vary substantially, the difference between rise times never exceeding 0.77 ms. Thus the multiple CFs contacting a mutant PC in this model share the same functional dendritic compartment.

We next asked whether the adult multi-innervation observed in the mutant mice represented an early-stage arrest of the developmental synapse-elimination process or abnormal reinnervation by additional CFs. Because developmental synapse elimination is necessary for the refinement of normal olivocerebellar topography (Fuhrman et al., 1994), we evaluated the distribution of anterogradely labeled CF axons in adult mutant mice. Despite the presence of multi-innervation, the topographic distribution of labeled CFs was consistent with the location of the olivary injections (data not shown) in accordance with known olivocerebellar topography (Sugihara and Shinoda, 2004), suggesting that olivocerebellar topography had undergone normal developmental regression and that multi-innervation was the result of subsequent local CF sprouting.

To verify this, we recorded from PCs of mutant animals and their control littermates at P15-P16, an age at which normal developmental synapse elimination is nearly complete (Fig. 10*E*). We found that 87.5% of mutant PCs ($N = 16$ cells, $n = 3$ animals) were mono-innervated at this age, compared with 75% of control littermate PCs ($N = 16$ cells, $n = 3$ animals); this difference is not statistically significant. Thus, mutant PCs appear to undergo a normal process of synapse elimination during development, and are contacted later by additional CFs once RORα is no longer expressed.

Injection of Cre-expressing lentivirus in adult *rora*$^{fl/fl}$ cerebellum

To verify that *rora* deletion in our model did not alter some late component of PC dendritic development, we examined the effect of *rora* deletion in adulthood. We injected LV-CMV-GFP (as a control) or LV-CMV-Cre lentiviral vectors into the cerebella of 2-month-old YFP*stop*$^{fl/fl}$;*rora*$^{fl/fl}$. The PC morphology was studied after survival times of either 2–4 weeks or 6 weeks. In LV-CMV-GFP–injected *rora*$^{fl/fl}$ mice, transduced PCs (GFP-immunoreactive) displayed normal morphology and VGLUT2 distribution on their dendrites (Fig. 11*D*). However, in LV-CMV-Cre–injected *rora*$^{fl/fl}$ mice, the few transduced PCs, as identified by the lack of an RORα-immunoreactive nucleus and either the expression of Calb1 (Fig. 11*A*,*B*) or the expression of YFP revealed by GFP immunohistochemistry (Fig. 11*C*), had VGLUT2-stained puncta around the soma

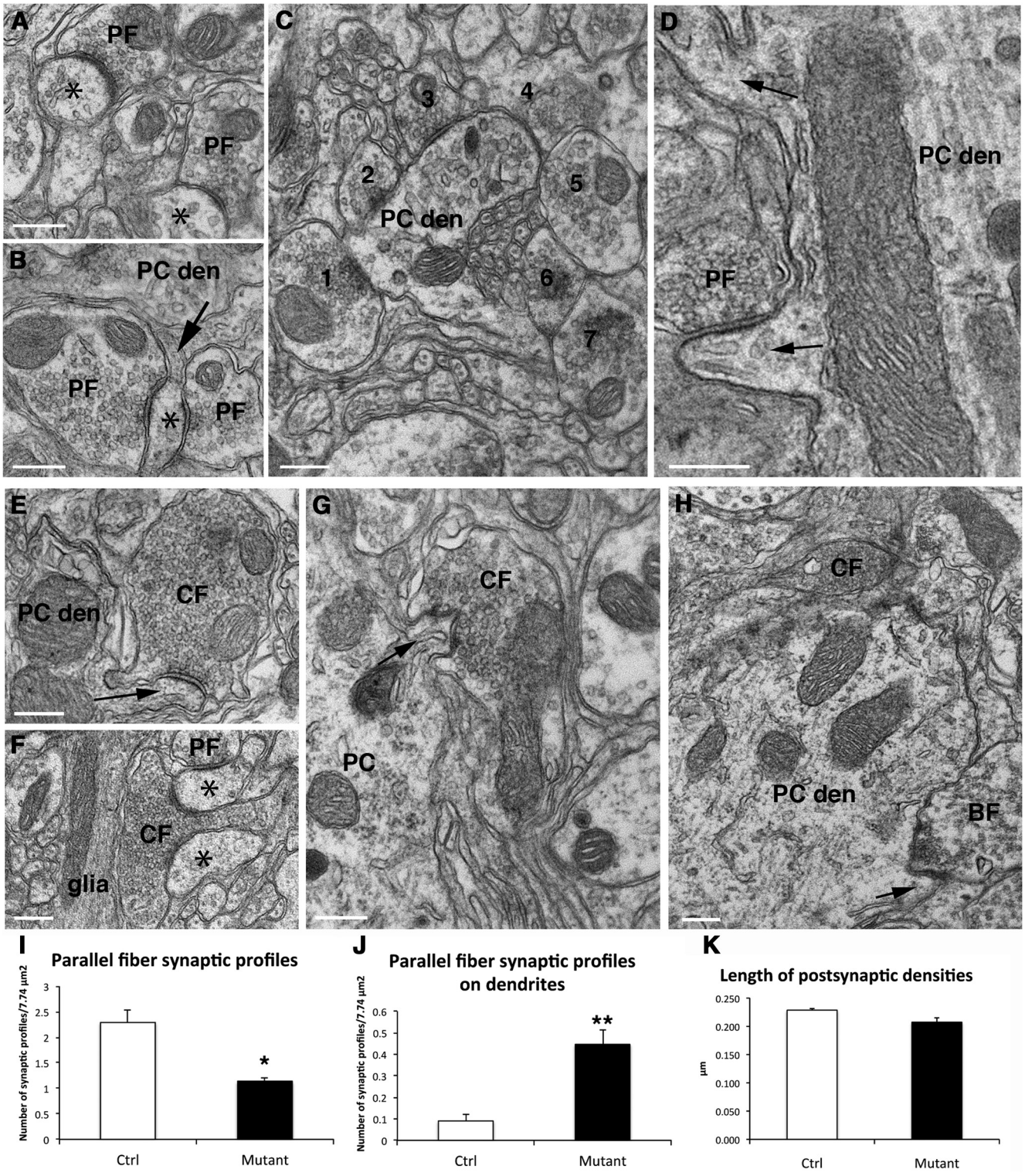

Figure 9. Electron micrographs of PFs (***A–D***) and CFs (***E–H***), on Purkinje cells of 2-month-old *rora* conditional mutant mice. ***A***, *Two PF varicosities establish synaptic contact with two Purkinje cell dendritic spines. There is presence of vesicular and tubular profiles of smooth endoplasmic reticulum within the spines. ***B***, *Two PF varicosities synapsing on the same dendritic spine. ***C***, Electron micrograph of a medium-sized Purkinje cell dendrite (PC den). The cytoplasm contains abundant profiles of smooth endoplasmic reticulum. This dendritic branch is devoid of spines, and seven PF varicosities (1–7) are in direct apposition with its surface, some of them establishing normal looking synaptic contacts with the smooth surface of the dendrite. ***D***, Large dendritic branch of a Purkinje cell (PC den). This stem dendrite is not smooth, and two spines (arrows) are emerging from it. The spine at the upper left corner of the micrograph is, in this plane of the section, free of innervation. In contrast, the lower spine is synapsing with a PF varicosity, indicating that PFs have invaded the dendritic domain normally reserved for CFs. ***E***, CF varicosity, identifiable by the large density of rounded synaptic vesicles, the presence of some large granulated vesicles and the electron density of the cytoplasmic matrix. The CF is in synaptic contact with a long-necked dendritic spine (arrow) belonging to a small-diameter Purkinje cell dendrite (PC den). ***F***, *CF varicosity synapsing on two Purkinje cell dendritic spines. Exceptionally, one of these spines is also in synaptic contact with a small PF varicosity. There is adjacent glial profile (glia), most probably belonging to a Bergmann fiber, filled with gliofilaments, indicating reactive gliosis. ***G***, CF varicosity in synaptic contact with a small somatic appendage (arrow) emerging from the cell body of a Purkinje cell. ***H***, Stem dendrite of a Purkinje cell (PC den) illustrating two classes of axon terminal climbing along the dendrite. The varicosity at the lower right corner belongs to a recurrent collateral of a basket cell axon (BF), and is straddling a small protrusion (arrow) on the smooth surface of the dendrite. (*Figure legend continues.*)

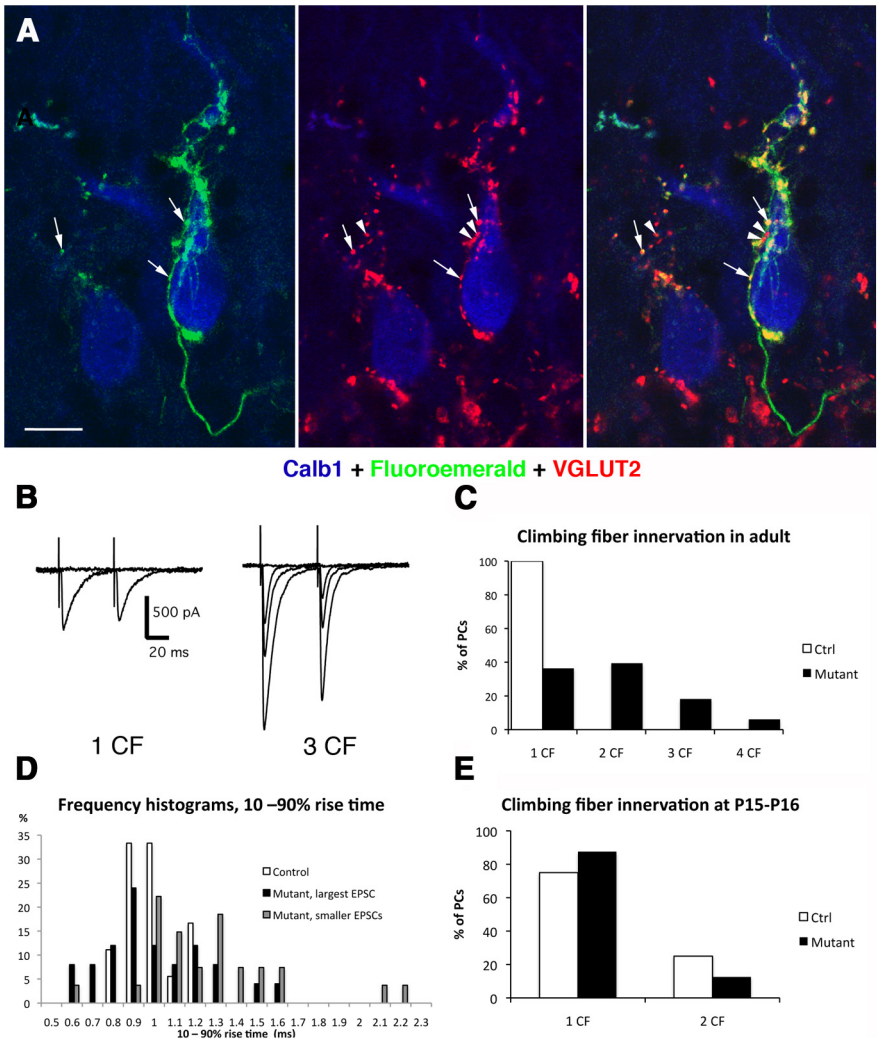

Figure 10. Multiple CF innervation of mutant Purkinje cells after deletion of *rora*. ***A***, Photomicrographs showing calbindin-immunolabeled Purkinje cells (blue) contacted by anterogradely labeled CFs (left) after injection of Fluoroemerald (green) into the inferior olive. Immunolabeling with VGLUT2 (red; middle) labels all CFs. The composite photomicrograph shows that at least two CFs contact these 2 PCs. Arrowheads indicate single-labeled CF (VGLUT2); arrows indicate double-labeled CF (VGLUT2, Fluoroemerald). Scale bar, 12 μm. ***B***, Examples of CF currents recorded in adult control PC (left) and a mutant PC (right). The control PC is contacted by a single CF; the mutant PC is contacted by three CFs. ***C***, Histogram showing the percentage of adult control (white bar) and mutant (black bars) PCs contacted by one or more CFs. $p < 0.001$ between the two groups (Fisher's exact test). ***D***, Frequency histogram showing the distribution of CF-EPSC rise times recorded in mutant and control PCs in the adult. There was no difference between the three groups (control CF-EPSCs; largest CF-EPSCs in the mutant; and smaller CF-EPSCs in the mutants; Fisher's exact test). ***E***, Histogram showing percentage of P15-P16 control PCs (white bars) and mutant PCs (black bars) showing CF mono-innervation or double innervation. There was no difference between the two groups (Fisher's exact test).

and the stem dendrites (Fig. 11*A–C*). Furthermore, although it is not clear whether the YFP completely filled the dendritic tree, transduced PCs appeared to have an atrophic dendritic tree (compare Fig. 11*C* with Fig. 11*D*). Quantitative analysis showed that more

←

(*Figure legend continued.*) At the upper part of the dendritic profile, there is a varicosity of a passing CF that does not establish synaptic contact at this plane of the section. The location of this CF could correspond to that of a CF at the "capuchon" stage. ***I***, Graphic representation of PF synaptic profiles per 7.74 μm^2. Error bars indicate SEM. *$p < 0.05$ between control (Ctrl) and mutant values (Student's *t* test). ***J***, Graphic representation of PF synaptic profiles on dendrites (identified by the presence of mitochondria) per 7.74 μm^2. Error bars indicate SEM. **$p < 0.01$ between control (Ctrl) and mutant values (Student's *t* test). ***K***, Graphic representation of length of postsynaptic densities. Error bars indicate SEM. No difference was detected between control (Ctrl) and mutant values. Scale bars, 250 nm.

rora$^{fl/fl}$ PCs transduced with LV-CMV-Cre present an increased number of VGLUT2 puncta on their soma or on their stem dendrites compared with PCs transduced with the control lentiviral vector (LV-CMV-GFP; Fig. 11*E*,*F*). These morphological modifications are very similar to those obtained with mutant (*Pcp2*::Cre$^{+/-}$; *Rora*$^{fl/fl}$) mice and confirm that RORα expression in the adult has a role in maintaining appropriately distributed CF synaptic innervation.

Discussion

In the cerebellum, RORα is expressed in PCs and molecular layer interneurons during development and through adulthood (Ino, 2004). Although its role in early development has been studied in *staggerer* mice and more recently using lentiviral vectors (for review, see Boukhtouche et al., 2006a), these previous studies did not address the potential role of ongoing RORα expression in the adult.

In this study, we used Cre-lox technology to delete *rora* specifically from PCs at ~2 weeks postnatal, an age when these neurons have passed the period of developmental neuronal death; they have an elaborate dendritic arbor; and most are innervated by a single CF, following the developmental process of multiinnervation and synapse elimination (for review, see Sotelo and Dusart, 2009; Kano and Hashimoto, 2009). Deletion of *rora* from PCs after P10 induced morphological regression of the dendritic arbor, the loss of distal spiny branchlets, the reestablishment of CF multiple innervation along with their perisomatic and basal stem dendritic relocation, and the death of some PCs, in association with a loss of motor coordination. Deletion of *rora* in the adult using lentiviral Cre induced a similar relocation of CFs to the perisomatic and basal dendritic compartment. These results show that, in addition to the well-known roles of RORα during early development, this transcription factor is necessary for the maintenance of normal characteristics in the adult PC shape and connectivity.

Our data show that late *rora* deletion is associated with a loss of 30% of PCs at 2-month-old. It has been previously shown that RORα haploinsufficiency seems to render PCs more vulnerable, as heterozygous *staggerer* mutants progressively lose 30% of their PCs between the ages of 3–12 months (Zanjani et al., 1992; Hadj-Sahraoui et al., 1997; Doulazmi et al., 1999; Janmaat et al., 2011). Thus, the PC loss we observed is similar to what is seen in models of RORα haploinsufficiency. Rates of PC loss were similar in the anterior and posterior lobes, although anterior lobes lost RORα expression before posterior lobes, indicating that there is no direct relation between PC maturation at the time of *rora* deletion

and PC death. Furthermore, at the electron microscopic level, we did not detect signs of ongoing degeneration. These observations support the proposal that RORα is a protective agent rather than a survival factor for PCs in adulthood, possibly by providing neuroprotection against reactive oxygen species-induced apoptosis (Boukhtouche et al., 2006c) and steroid hormone deficiency (Jan-maat et al., 2011). Our data indicate that the absence of RORα will progressively increase the risk of cell death over time, depending on the accumulated insults received by PCs.

One clear result of the loss of RORα in this model is a striking reduction of the dendritic tree and torpedo axon modifications, suggesting regressive events. The normal PC dendritic tree is compartmentalized into a proximal compartment, composed of thick dendritic branches, giving rise to the distal compartment of the spiny branchlets. The proximal compartment is the postsynaptic domain for CFs (on small rounded spines, the thorns); the distal compartment is contacted by PFs (on spines of the tertiary branchlets) (for review, see Cesa and Strata, 2009). RORα haploinsufficiency is associated with premature dendritic atrophy from 4 months of age (Hadj-Sahraoui et al., 2001). However, in that model, the haploinsufficiency is present throughout life, and it is thus not possible to determine whether this dendritic atrophy is simply a delayed effect of abnormal development. Here, with the removal of *rora* after substantial development of the dendritic tree, we observed a significant decrease of the size of the arborization 6 weeks after *rora* deletion at P30. This indicates that the atrophy in the previously studied haploinsufficient mice may well be the result of a need for RORα in the adult to maintain the dendritic tree, rather than a developmental phenomenon. Thus, in addition to its role in the initial development of the dendritic tree (Boukhtouche et al., 2006b), RORα also seems to be required for dendritic maintenance throughout life.

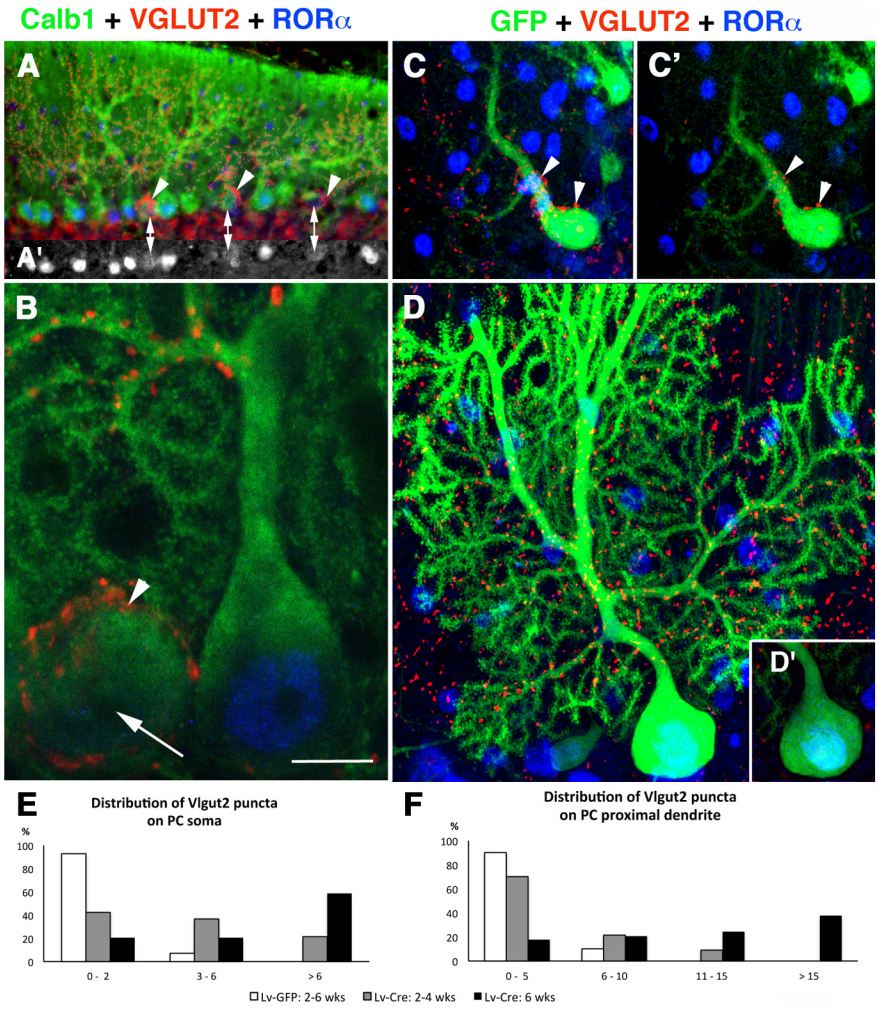

Figure 11. Effect of adult *rora* deletion. ***A***, ***B***, Photomicrograph (***A***) and confocal image (***B***) of vermis parasagittal cerebellar sections triple-immunostained for Calb1 (green), VGLUT2 (red), and RORα (blue) from 2-month-old *Pcp2*::Cre$^{-/-}$;*Rora*$^{fl/fl}$ injected with Cre lentiviral vector with a 2 week survival time. ***A′***, The RORα staining at the level of the PC nucleus is presented in black and white. Double-head arrows point to the same PC nuclei between ***A*** and ***A′***. Arrows indicate the presence of VGLUT2 puncta. ***B***, The transduced Purkinje cell (lacking an RORα-immunoreactive nucleus, arrow) presents VGLUT2-immunoreactive puncta (arrowhead) around its soma. ***C***, ***D***, Maximal projections from stacks of confocal images of vermis parasagittal cerebellar sections triple-immunostained for GFP (green), VGLUT2 (red), and RORα (blue) from 2-month-old YFP*stop*$^{fl/fl}$;*Rora*$^{fl/fl}$ injected with Cre lentiviral vector (***C***) or GFP lentiviral vector (***D***) with a 6 week survival time. ***C′***, ***D′***, Confocal images from the stack used to make images in ***C*** and ***D***, respectively. The magnification is the same in ***C*** and ***D***, indicating that the *rora*-depleted PC is atrophic. The transduced Purkinje cells (lacking an RORα-immunoreactive nucleus, arrows) present VGLUT2-immunoreactive puncta (arrowheads) either around their soma or on the stem part of their main dendritic branch (***C***,***C′***), whereas a control PC (***D***,***D′***) does not. Scale bars: ***A***, 100 μm; ***B***, 10 μm; ***C***, ***C′***, ***D***, ***D′***, 20 μm. ***E***, ***F***, Histograms showing the percentage of PCs transduced with LV-CMV-GFP (white bar; control vector), or LV-CMV-Cre with 2 week to 4 week survival time (gray bars) or 6 week survival time (black bars) contacted by more or fewer VGLUT2 puncta on soma (***E***) and the stem dendrite (***F***). The number of VGLUT2 puncta directly apposed to the soma or to the stem dendrite (first 20 μm from the cell body) were counted throughout the stack of images. In both cases, $p < 0.001$ (Fisher's exact test).

Our results further show that the reduction of the dendritic tree is not simply the result of nonspecific dendritic atrophy. In 30% of the analyzed cells (the "small PCs"), mutant PCs were reduced in size but had a dendritic complexity near to control. These small PCs have reduced dendritic tree height but not width compared with control PCs. It is interesting to recall that, during rat PC development, dendrite growth occurs first mainly in sagittal direction, reaching its full width by P15, and then in height (Berry and Bradley, 1976). Thus, at least for some PCs, the dendritic tree degeneration process appears to be the reverse of the developmental pattern.

Adult mutant PCs had many fewer spiny branchlets than P15 mutant PCs, suggesting that dendritic spiny branchlets are lost rather than failing to develop. In addition, spiny branchlets are also absent from quite complex dendritic tree (small PCs), indicating that branchlet loss precedes, and might be independent of, branch retraction. It is known that, if RORα is absent throughout development, the surviving PCs lack spiny branchlets and PF synapses (Sotelo and Changeux, 1974; Landis and Sidman, 1978). However, the multiple developmental roles of RORα complicate the analysis of its role in the formation and maintenance of spines. Nevertheless, numerous observations from both normal and abnormally developed cerebella indicate that the formation

of PC tertiary spines does not depend on presynaptic PF axons but are likely to be an intrinsic property of the neuron (Sotelo, 1978; Yuste and Bonhoeffer, 2004). The experimental model described here allows us to delete *rora* in a relatively mature PC. The observation that these PCs then lose most of their distal spines despite the presence of PF terminals on PC dendrites leads us to propose that *rora* may be one of the important factors in the maintenance of PC distal spines throughout life.

In addition to these regressive events, late removal of *rora* from PCs induces three immature characteristics. First, these PCs present a higher level of FOXP2 immunoreactivity compared with control. This is consistent with reacquisition of PC immaturity because it is known that FOXP2 expression decreases in PCs as development proceeds (Ferland et al., 2003; Schüller et al., 2006). Second, in both mutant and virally transduced mature PCs, the location of CFs resembles the immature "capuchon" stage (Ramón y Cajal, 1911; Chédotal and Sotelo, 1993; Watanabe and Kano, 2011). Similar patterns of abnormal CF location were described in several spontaneous mouse mutations affecting the cerebellum (Rossi et al., 1995); the CF morphology reflects preceding interactions with their postsynaptic neurons and is determined by the age of onset and progression of PC degeneration.

Third, in addition to the abnormal CF localization, we observed a return to multi-innervation of PCs by CFs. To our knowledge, the only other clear reestablishment of multiple CF innervation (as opposed to a persistence of developmental multi-innervation) has been observed in the case of late deletion of GluRδ2 (Miyazaki et al., 2010). GluRδ2 is involved in the maintenance of PF/PC synapses (Takeuchi et al., 2005). In the mouse model of GluRδ2 ablation in adult PCs, Miyazaki et al. (2010) showed that this receptor is a key element for maintaining CF mono-innervation, likely by preventing the sprouting of these fibers and their invasion of PF sites on nearby PCs. Indeed, considerable evidence suggests that the distribution of innervation territory on the PC dendrites results from heterosynaptic competition between PFs and CFs (Cesa and Strata, 2009). In the absence of RORα, the process of new CF multi-innervation is very different: the CFs, instead of invading the PF territory, return to the immature perisomatic net and "capuchon" stages (Ramón y Cajal, 1911; Chédotal and Sotelo, 1992; Watanabe and Kano, 2011). Nevertheless, the regressive morphological processes that these PC dendritic trees undergo, by suppressing the vast majority of tertiary spines, create an abnormal situation for adult PCs in which the partition of dendritic territory between PFs and CFs is disturbed. This situation is similar to that described for PC-$Ca_v2.1$ KO mice, in which the extent of CF territory was limited to the soma and basal dendrites, whereas PF territory was expanded (Miyazaki et al., 2012). However, in late *rora*-deleted PCs, we do not observe the hyperspiny transformation of the PC proximal somatodendritic domain to the extent described in PC-$Ca_v2.1$ mutants. Further work is necessary to understand the different mechanisms involved in heterosynaptic competition between PFs and CFs and homosynaptic competition among multiple CFs (Watanabe and Kano, 2011).

Thus, the loss of RORα in mature PCs induces the reacquisition of several immature characteristics, suggesting that this transcription factor is important for the maintenance of the mature differentiation stage of PCs. We propose that RORα is a terminal differentiation gene as defined by Hobert (2011), that is, part of the program that defines the functional properties of a mature PC throughout its life.

References

Berry M, Bradley P (1976) The growth of the dendritic trees of Purkinje cells in the cerebellum of the rat. Brain Res 112:1–35. CrossRef Medline

Boukhtouche F, Doulazmi M, Frederic F, Dusart I, Brugg B, Mariani J (2006a) RORα, a pivotal nuclear receptor for Purkinje neuron survival and differentiation: from development to ageing. Cerebellum 5:97–104. CrossRef Medline

Boukhtouche F, Janmaat S, Vodjdani G, Gautheron V, Mallet J, Dusart I, Mariani J (2006b) Retinoid-related orphan receptor α controls the early steps of Purkinje cell dendritic differentiation. J Neurosci 26:1531–1538. CrossRef Medline

Boukhtouche F, Vodjdani G, Jarvis CI, Bakouche J, Staels B, Mallet J, Mariani J, Lemaigre-Dubreuil Y, Brugg B (2006c) Human retinoic acid receptor-related orphan receptor α1 overexpression protects neurones against oxidative stress-induced apoptosis. J Neurochem 96:1778–1789. CrossRef Medline

Cesa R, Strata P (2009) Axonal competition in the synaptic wiring of the cerebellar cortex during development and in the mature cerebellum. Neurosci 162:624–632. CrossRef Medline

Chan-Palay V, Palay SL (1970) Interrelations of basket cell axons and climbing fibers in the cerebellar cortex of the rat. Z Anat Entwicklungsgesch 132:191–227. CrossRef Medline

Chédotal A, Sotelo C (1992) Early development of olivocerebellar projections in the fetal rat using CGRP immunocytochemistry. Eur J Neurosci 4:1159–1179. CrossRef Medline

Chédotal A, Sotelo C (1993) The "creeper stage" in cerebellar climbing fiber synaptogenesis precedes the "pericellular nest": ultrastructural evidence with parvalbumin immunocytochemistry. Brain Res Dev Brain Res 76: 207–220. CrossRef Medline

Crepel F, Delhaye-Bouchaud N, Guastavino JM, Sampaio I (1980) Multiple innervation of cerebellar Purkinje cells by climbing fibres in staggerer mutant mouse. Nature 283:483–484. CrossRef Medline

Dixon KJ, Sherrard RM (2006) Brain-derived neurotrophic factor induces post-lesion transcommissural growth of olivary axons that develop normal climbing fibers on mature Purkinje cells. Exp Neurol 202:44–56. CrossRef Medline

Doulazmi M, Frédéric F, Lemaigre-Dubreuil Y, Hadj-Sahraoui N, Delhaye-Bouchaud N, Mariani J (1999) Cerebellar Purkinje cell loss during life span of the heterozygous staggerer mouse (Rora(+)/Rora(sg)) is gender-related. J Comp Neurol 411:267–273. CrossRef Medline

Doulazmi M, Frederic F, Capone F, Becker-Andre M, Delhaye-Bouchaud N, Mariani J (2001) A comparative study of Purkinje cells in two RORα gene mutant mice: staggerer and RORα(−/−). Dev Brain Res 127:165–174. CrossRef Medline

Dusart I, Sotelo C (1994) Lack of Purkinje cell loss in adult rat cerebellum following protracted axotomy: degenerative changes and regenerative attempts of the severed axons. J Comp Neurol 347:211–232. CrossRef Medline

Dussault I, Fawcett D, Matthyssen A, Bader JA, Giguère V (1998) Orphan nuclear receptor ROR α-deficient mice display the cerebellar defects of staggerer. Mech Dev 70:147–153. CrossRef Medline

Ferland RJ, Cherry TJ, Preware PO, Morrisey EE, Walsh CA (2003) Characterization of Foxp2 and Foxp1 mRNA and protein in the developing and mature brain. J Comp Neurol 460:266–279. CrossRef Medline

Fuhrman Y, Thomson MA, Piat G, Mariani J, Delhaye-Bouchaud N (1994) Enlargement of olivo-cerebellar microzones in the agranular cerebellum of adult rats. Brain Res 638:277–284. CrossRef Medline

Hadj-Sahraoui N, Frederic F, Zanjani H, Herrup K, Delhaye-Bouchaud N, Mariani J (1997) Purkinje cell loss in heterozygous staggerer mutant mice during aging. Dev Brain Res 98:1–8. CrossRef Medline

Hadj-Sahraoui N, Frederic F, Zanjani H, Delhaye-Bouchaud N, Herrup K, Mariani J (2001) Progressive atrophy of cerebellar Purkinje cell dendrites during aging of the heterozygous staggerer mouse (Rora(+/sg)). Dev Brain Res 126:201–209. CrossRef Medline

Hamilton BA, Frankel WN, Kerrebrock AW, Hawkins TL, FitzHugh W, Kusumi K, Russell LB, Mueller KL, van Berkel V, Birren BW, Kruglyak L, Lander ES (1996) Disruption of the nuclear hormone receptor RORα in staggerer mice. Nature 379:736–739. CrossRef Medline

Heck N, Betuing S, Vanhoutte P, Caboche J (2012) A deconvolution method to improve automated 3D-analysis of dendritic spines: application to a mouse model of Huntington's disease. Brain Struct Funct 217: 421–434. CrossRef Medline

Herrup K, Mullen RJ (1979) Regional variation and absence of large neurons in the cerebellum of the *staggerer* mouse. Brain Res 172:1–12. CrossRef Medline

Hobert O (2011) Regulation of terminal differentiation programs in the nervous system. Annu Rev Cell Dev Biol 27:681–696. CrossRef Medline

Ino H (2004) Immunohistochemical characterization of the orphan nuclear receptor RORα in the mouse nervous system. J Histochem Cytochem 52:311–323. CrossRef Medline

Janmaat S, Akwa Y, Doulazmi M, Bakouche J, Gautheron V, Liere P, Eychenne B, Pianos A, Luiten P, Groothuis T, Baulieu EE, Mariani J, Sherrard RM, Frederic F (2011) Age-related Purkinje cell death is steroid dependent: RORα haplo-insufficiency impairs plasma and cerebellar steroids and Purkinje cell survival. Age (Dordr) 33:565–578. CrossRef Medline

Kadkhodaei B, Ito T, Joodmardi E, Mattsson B, Rouillard C, Carta M, Muramatsu S, Sumi-Ichinose C, Nomura T, Metzger D, Chambon P, Lindqvist E, Larsson NG, Olson L, Björklund A, Ichinose H, Perlmann T (2009) Nurr1 is required for maintenance of maturing and adult midbrain dopamine neurons. J Neurosci 29:15923–15932. CrossRef Medline

Kano M, Hashimoto K (2009) Synapse elimination in the central nervous system. Curr Opin Neurobiol 19:154–161. CrossRef Medline

Konnerth A, Llano I, Armstrong CM (1990) Synaptic currents in cerebellar Purkinje cells. Proc Natl Acad Sci U S A 87:2662–2665. CrossRef Medline

Landis DM, Sidman RL (1978) Electron microscopic analysis of postnatal histogenesis in the cerebellar cortex of staggerer mutant mice. J Comp Neurol 179:831–863. CrossRef Medline

Larramendi EM, Victor T (1967) Synapses on Purkinje cell spines in the mouse: an electron microscopic study. Brain Res 5:15–30. CrossRef Medline

Letellier M, Bailly Y, Demais V, Sherrard RM, Mariani J, Lohof AM (2007) Reinnervation of late postnatal Purkinje cells by climbing fibers: neosynaptogenesis without transient multi-innervation. J Neurosci 27:5373–5383. CrossRef Medline

Liu C, Maejima T, Wyler SC, Casadesus G, Herlitze S, Deneris ES (2010) Pet-1 is required across different stages of life to regulate serotonergic function. Nat Neurosci 13:1190–1198. CrossRef Medline

Mariani J, Changeux JP (1980) Multiple innervation of Purkinje cells by climbing fibers in the cerebellum of the adult staggerer mutant mouse. J Neurobiol 11:41–50. CrossRef Medline

Miyazaki T, Watanabe M (2011) Development of an anatomical technique for visualizing the mode of climbing fiber innervation in Purkinje cells and its application to mutant mice lacking GluRδ2 and Ca(v)2.1. Anat Sci Int 86:10–18. CrossRef Medline

Miyazaki T, Fukaya M, Shimizu H, Watanabe M (2003) Subtype switching of vesicular glutamate transporters at parallel fibre–Purkinje cell synapses in developing mouse cerebellum. Eur J Neurosci 17:2563–2572. CrossRef Medline

Miyazaki T, Yamasaki M, Takeuchi T, Sakimura K, Mishina M, Watanabe M (2010) Ablation of glutamate receptor GluRδ2 in adult Purkinje cells causes multiple innervation of climbing fibers by inducing aberrant invasion to parallel fiber innervation territory. J Neurosci 30:15196–15209. CrossRef Medline

Miyazaki T, Yamasaki M, Hashimoto K, Yamazaki M, Abe M, Usui H, Kano M, Sakimura K, Watanabe M (2012) Cav2.1 in cerebellar Purkinje cells regulates competitive excitatory synaptic wiring, cell survival, and cerebellar biochemical compartmentalization. J Neurosci 32:1311–1328. CrossRef Medline

Palay SL, Chan-Palay V (1974) Cerebellar cortex: cytology and organization. New York: Springer.

Polleux F, Ince-Dunn G, Ghosh A (2007) Transcriptional regulation of vertebrate axon guidance and synapse formation. Nat Rev Neurosci 8:331–340. CrossRef Medline

Ramón y Cajal S (1911) Histologie du Système Nerveux de l'Homme et des Vertébrés, Vol. 2. Maloine: Paris.

Rasband WS (2008) ImageJ, 1997–2008. Bethesda, MD: U.S. National Institutes of Health. http://rsb.info.nih.gov/ij/.

Rodriguez A, Ehlenberger DB, Dickstein DL, Hof PR, Wearne SL (2008) Automated three-dimensional detection and shape classification of dendritic spines from fluorescence microscopy images. PloS One 3:e1997. CrossRef Medline

Rondi-Reig L, Mariani J (2002) To die or not to die, does it change the function? Behavior of transgenic mice reveals a role for developmental cell death. Brain Res Bull 57:85–91. CrossRef Medline

Rondi-Reig L, Lohof A, Dubreuil YL, Delhaye-Bouchaud N, Martinou JC, Caston J, Mariani J (1999) Hu-Bcl-2 transgenic mice with supernumerary neurons exhibit timing impairment in a complex motor task. Eur J Neurosci 11:2285–2290. CrossRef Medline

Rondi-Reig L, Lemaigre-Dubreuil Y, Montecot C, Muller D, Martinou JC, Caston J, Mariani J (2001) Transgenic mice with neuronal overexpression of bcl-2 gene present navigation disabilities in a water task. Neurosci 104:207–215. CrossRef Medline

Rondi-Reig L, Arabo A, Leboucher P, Rateau S, Dupraz Y (2008) Evaluation automatique des capacités de coordination motrices chez la souris. No. DI 01873–01. France.

Rossi F, Jankovski A, Sotelo C (1995) Target neuron controls the integrity of afferent axon phenotype: a study on the Purkinje cell-climbing fiber system in cerebellar mutant mice. J Neurosci 15:2040–2056. Medline

Schüller U, Kho AT, Zhao Q, Ma Q, Rowitch DH (2006) Cerebellar "transcriptome" reveals cell-type and stage-specific expression during postnatal development and tumorigenesis. Mol Cell Neurosci 33:247–259. CrossRef Medline

Scorcioni R, Polavaram S, Ascoli GA (2008) L-Measure: a web-accessible tool for the analysis, comparison and search of digital reconstructions of neuronal morphologies. Nat Protoc 3:866–876. CrossRef Medline

Sherrard RM, Bower AJ, Payne JN (1986) Innervation of the adult rat cerebellar hemisphere by fibres from the ipsilateral inferior olive following unilateral neonatal pedunculotomy: an autoradiographic and retrograde fluorescent double-labelling study. Exp Brain Res 62:411–421. Medline

Sotelo C (1975) Dendritic abnormalities of Purkinje cells in the cerebellum of the neurological mutant mice (*weaver* and *staggerer*). In: Advances in neurology, Vol 12: Physiology and pathology of dendrites (GW Kreutzberg, ed), 335–351. New York: Raven.

Sotelo C (1978) Purkinje cell ontogeny: formation and maintenance of spines. Prog Brain Res 48:149–170. CrossRef Medline

Sotelo C, Changeux JP (1974) Transsynaptic degeneration "en cascade" in the cerebellar cortex of staggerer mutant mice. Brain Res 67:519–526. CrossRef Medline

Sotelo C, Dusart I (2009) Intrinsic versus extrinsic determinants during the development of Purkinje cell dendrites. Neuroscience 162:589–600. CrossRef Medline

Sotelo C, Hillman DE, Zamora AJ, Llinás R (1975) Climbing fiber deafferentation: its action on Purkinje cell dendritic spines. Brain Res 98:574–581. CrossRef Medline

Srinivas S, Watanabe T, Lin CS, William CM, Tanabe Y, Jessell TM, Costantini F (2001) Cre reporter strains produced by targeted insertion of EYFP and ECFP into the ROSA26 locus. BMC Dev Biol 1:4. CrossRef Medline

Sugihara I (2006) Organization and remodeling of the olivocerebellar climbing fiber projection. Cerebellum 5:15–22. CrossRef Medline

Sugihara I, Shinoda Y (2004) Molecular, topographic, and functional organization of the cerebellar cortex: a study with combined aldolase C and olivocerebellar labeling. J Neurosci 24:8771–8785. CrossRef Medline

Sugihara I, Lohof AM, Letellier M, Mariani J, Sherrard RM (2003) Post-lesion transcommissural growth of olivary climbing fibres creates functional synaptic microzones. Eur J Neurosci 18:3027–3036. CrossRef Medline

Takei K, Mignery GA, Mugnaini E, Südhof TC, De Camilli P (1994) Inositol 1,4,5-trisphosphate receptor causes formation of ER cisternal stacks in transfected fibroblasts and in cerebellar Purkinje cells. Neuron 12:327–342. CrossRef Medline

Takeuchi T, Miyazaki T, Watanabe M, Mori H, Sakimura K, Mishina M (2005) Control of synaptic connection by glutamate receptor δ2 in the adult cerebellum. J Neurosci 25:2146–2156. CrossRef Medline

van Welie I, Smith IT, Watt AJ (2011) The metamorphosis of the developing cerebellar microcircuit. Curr Opin Neurobiol 21:245–253. CrossRef Medline

Vogel MW, Sinclair M, Qiu D, Fan H (2000) Purkinje cell fate in staggerer mutants: agenesis versus cell death. J Neurobiol 42:323–337. CrossRef Medline

Watanabe M, Kano M (2011) Climbing fiber synapse elimination in cerebellar Purkinje cells. Eur J Neurosci 34:1697–1710. CrossRef Medline

Yuste R, Bonhoeffer T (2004) Genesis of dendritic spines: insights from ul-

trastructural and imaging studies. Nat Rev Neurosci 5:24–34. CrossRef Medline

Zanjani HS, Mariani J, Delhaye-Bouchaud N, Herrup K (1992) Neuronal cell loss in heterozygous staggerer mutant mice: a model for genetic contributions to the aging process. Dev Brain Res 67:153–160. CrossRef Medline

Zennou V, Serguera C, Sarkis C, Colin P, Perret E, Mallet J, Charneau P (2001) The HIV-1 DNA flap stimulates HIV vector-mediated cell transduction in the brain. Nat Biotechnol 19:446–450. CrossRef Medline

Zufferey R, Nagy D, Mandel RJ, Naldini L, Trono D (1997) Multiply attenuated lentiviral vector achieves efficient gene delivery in vivo. Nat Biotechnol 15:871–875. CrossRef Medline